Petroleum Science 19 (2022) 2583–2600

Contents lists available at ScienceDirect

Petroleum Science

journal homepage: www.keaipublishing.com/en/journals/petroleum-science

Original Paper

# Overpressure and gas charging in tight sandstone: Xujiahe Formation, northeastern Sichuan Basin

Jing-Dong Liu [a, b, c, *], Cun-Jian Zhang [c], You-Lu Jiang [a, b, c], Guo-Shuai Bai [c]

[a] Shandong Provincial Key Laboratory of Deep Oil and Gas, China University of Petroleum (East China), Qingdao, Shandong, 266580, China
[b] Shandong Provincial Key Laboratory of Reservoir Geology, China University of Petroleum (East China), Qingdao, Shandong, 266580, China
[c] School of Geosciences, China University of Petroleum (East China), Qingdao, Shandong, 266580, China

ARTICLE INFO

*Article history:*
Received 26 February 2022
Received in revised form
8 June 2022
Accepted 17 August 2022
Available online 22 August 2022

Edited by Jie Hao and Teng Zhu

*Keywords:*
Tight sandstone gas
Overpressure
Hydrocarbon generation
Tectonic compression
Driving force for tight gas charging
Sichuan Basin

ABSTRACT

Overpressure is a key factor for oil and gas charging in tight reservoirs, but it is still a challenge to evaluate the overpressure evolution and its control on oil and gas charging. Taking Xujiahe Formation in the northeastern Sichuan Basin as an example, this paper presented a method for evaluating overpressure and its effect on natural gas charging in tight sandstone in compressional basin. The abnormally high pressure and its causes were analyzed by measured data and logging evaluation. Theoretical calculation and PVT simulation were used to investigate the amounts of overpressure resulted from hydrocarbon generation and tectonic compression, respectively. Then the source rock - reservoir pressure differences were calculated and the characteristics of natural gas charging during the natural gas charging periods were analyzed. It was revealed that hydrocarbon generation and tectonic compression were the main causes of the overpressure. The overpressure of both source rocks and reservoir exhibited a gradually increasing trend from Middle Jurassic to Early Cretaceous ($J_2$-$K_1$), then decreased since Later Cretaceous ($K_2$), and some of that preserved to now. The contributions of the hydrocarbon generation and tectonic compression to overpressure were different in different periods. The residual pressure difference between the source rocks and the reservoir is the major driving force for tight sandstone gas charging. The main hydrocarbon generating area of the source rocks and the area of high driving force were major natural gas enrichment areas, and the driving force determined the natural gas charging space in the pore throat system of the reservoir. This research helps evaluate the overpressure and pressure difference between source rocks and reservoir in compressed basin, as well as investigate the effective pore throat space of tight gas charging by the driver of overpressure.


## 1. Introduction

As an unconventional resource, tight sandstone gas is mainly stored in sandstone reservoirs with an overburden pressure permeability $\leq 0.1 \times 10^{-3}$ μm$^2$ (air permeability $\leq 1 \times 10^{-3}$ μm$^2$) (Rezaee et al., 2012; Xu, 2017). As an important field of petroleum exploration, tight sandstone gas has been discovered or speculated to be developed in about 70 basins around the world (Rogner, 1997; Dai et al., 2012; Shanley and Cluff, 2015), with a resource amount of $210 \times 10^{12}$ m$^3$ (Yang et al., 2012). Taking United States and China as cases, the productions of tight sandstone gas have accounted for 30% of their total domestic natural gas productions (Yu et al., 2015). Furthermore, tight sandstone gas will account for an even greater proportion of new natural gas reserves in the future (Wei et al., 2017).

Tight sandstone gas has characteristics of tight reservoir, abnormal formation pressure, source-reservoir proximity, and large-area distribution (Liu et al., 2015; Wu et al., 2017; Tong et al., 2012). In contrast to conventional reservoir, tight sandstone mainly develops nano-micro pore throat networks (Krakowska et al., 2018; Bera and Shah, 2021; Liu et al., 2022a, 2022b), and relatively large capillary resistance needs to be overcome for natural gas migration (Shanley and Cluff, 2015). Through theoretical analysis and physical simulation experiments, many scholars believed that the overpressure was the major driving force for hydrocarbon migration (Law and Curtis, 2002; Li and Li, 2010; Zhang et al., 2012; Jia et al.,

* Corresponding author. Shandong Provincial Key Laboratory of Deep Oil and Gas, China University of Petroleum (East China), Qingdao, Shandong 266580, China.
*E-mail address:* liujingdong@upc.edu.cn (J.-D. Liu).

https://doi.org/10.1016/j.petsci.2022.08.023

2012; Liu et al., 2021), and hydrocarbon migration had the characteristic of low-speed non-Darcy flow (Kuhn et al., 2012; Tao et al., 2016). The residual pressure difference between source rock and reservoir during the hydrocarbon charging period was the driving force for tight oil and gas charging into the tight reservoir, whose accuracy depends on the restoration of paleo-pressure of the reservoir and its adjacent source rocks. The restoration of paleo-pressure is further closely related to the identification of the causes of the overpressure. However, due to factors such as diverse types of basins, differences in tectonic and sedimentary evolution, the causes for overpressure in different basins or different areas of one basin often differ greatly (Meckel and Thomasson, 2005). The identification of the causes for overpressure and the restoration of paleo-pressure are currently key problems that need to be solved urgently.

Sichuan Basin, as a compressional basin, is one of the key basins for conventional and unconventional natural gas exploration and development in China (Xu et al., 2011; Dong et al., 2014). The Upper Triassic Xujiahe Formation of Sichuan Basin is enrichment in tight sandstone gas (Ma et al., 2012; Yue et al., 2018). In recent years, the exploration and development of the Xujiahe Formation in northeastern Sichuan Basin has witnessed major breakthroughs and proved great exploration potential (Dai et al., 2009; Qin et al., 2018). Drilling revealed that some wells have obtained high-yield industrial gas flow in the Xujiahe Formation, but there are also some wells with poor drilling results. How to explain this phenomenon on hydrocarbon enrichment difference is a difficult problem. Nowadays, few studies were conducted on the overpressure causes and the driving force for tight sandstone gas charging, restricting in-depth understanding of the reasons of the gas accumulation and distribution.

The tight sandstone gas of Xu-4 member of Xujiahe Formation in northeastern Sichuan Basin was taken as an example. The main problems to be solved in this paper include: (1) Identifying the causes for overpressure and restoring the paleo-pressure evolution of reservoir and its adjacent source rocks. (2) Calculating the source-reservoir pressure differences during the critical charging periods (i.e., the driving force for natural gas charging), and analyzing their effects on natural gas charging. This research will be helpful to improve the evaluation methods of overpressure and source-reservoir overpressure difference in compressional basin, as well as investigate the role of driving force in tight sandstone gas charging. It is also important to understand the mechanisms of natural gas migration and accumulation and predict favorable exploration zones.

## 2. Geologic setting

Sichuan Basin is the second largest petroliferous basin in China (Zheng et al., 2019), located on the eastern edge of the Qinghai-Tibet Plateau on the basis of the Upper Yangtze Craton (Wang et al. 2014, 2018). The northeastern part of Sichuan Basin is a low and gentle tectonic area at the intersection of Dabashan thrust nappe belt, Micangshan uplift tectonic belt and Longmenshan tectonic belt (Fig. 1). Its tectonic units include Tongnanba anticline, Tongjiang depression, southwestern of Chixi depression, southwestern of Jiulongshan anticline, and Cangxi-Bazhong low and gentle structural belt. Since Xujiahe Formation sedimentation, it has mainly experienced three periods of tectonic compression (Yokoyama et al., 2001; Jin et al., 2009; Shen et al., 2009): (1) Uplift from the Middle Jurassic to Late Jurassic caused by the Indosinian movement, (2) strong uplift and fault development in the Late Cretaceous caused by the late Yanshan movement, and (3) another strong uplift and eastern fault development during Paleogene Eocene-Oligocene due to the Himalayan movement.

From Sinian to Cretaceous, the study area had undergone a sedimentary evolution process from marine facies, marine-continental transitional facies to continental facies (Ma et al., 2007). The Xujiahe Formation of Upper Triassic is a typical continental clastic rock deposit with marine-continental transitional facies (Guo et al., 2015). The Xujiahe Formation can be divided into Xu-1, Xu-2, Xu-3, Xu-4, Xu-5 members from bottom to top, with a cumulative thickness of up to 1 km. In which, Xu-1, Xu-3, and Xu-5 members are the main source rock layers, whose lithology is mainly dark mudstone, with locally developed carbonaceous mudstone and coal rock. The type of organic matter for these source rocks is partial humic, and the organic matter maturity has reached a high-over mature stage. Xu-2 and Xu-4 members are the main reservoirs with poor physical properties, the average porosity and permeability are 3.36% and 0.51 mD, respectively. The distribution of Xu-4 member on the plane in northeastern Sichuan Basin is wide and stable, and the rock types are lithic sandstone and feldspar lithic sandstones. Source rocks of Xu-3 member are generally developed, especially the ends of west and east of the study area. Source rock of Xu-5 member mainly distributed in the western regions, such as the areas of well YL171 and well YL173 (Fig. 2).

## 3. Methods

### 3.1. Research procedure

The procedure of this research was as follows. Firstly, the characteristics of current formation pressure and abnormally high pressure in Xujiahe Formation were analyzed, and the main causes of overpressure were analyzed by logging evaluation. Secondly, the period of natural gas charging in Xu-4 member reservoir was identified using the source rock hydrocarbon generation method and fluid inclusion method. Thirdly, using the methods of fluid inclusion PVT simulation and basin simulation, the pressure evolution of Xu-4 member reservoir was analyzed. The amounts of overpressure resulted from geological factors (hydrocarbon generation and tectonic compression) were calculated, which were used to analyze the pressure evolution of source rocks of the Xu-3 and Xu-5 members. Finally, the source rock - reservoir pressure differences were calculated (pressure difference between the Xu-3 and the Xu-4 members, as well as that between Xu-5 and Xu4-members) during the natural gas charging periods, thereby obtaining the driving force for natural gas charging.

### 3.2. Data and samples analyses

Drilling and logging data of the study area, including lithology, acoustic time difference logging, density logging, resistivity logging, physical property and measured formation pressure, were collected from Sinopec Exploration Company. Composition of natural gas in the reservoir, and total organic carbon (TOC), vitrinite reflectance (Ro) and hydrogen index (HI) of the source rocks were also collected. Core samples of Xu-4 member were used to make casting thin sections and fluid inclusion slices. Casting thin sections were used to observe the rock type and cement characteristics, and fluid inclusion slices were used to analyze the inclusion types and the homogenization temperatures (Th).

The observation of the casting thin sections and fluid inclusion slices were conducted using a ZEISS AXIO Imager D1m multifunctional research-grade microscope, which was equipped with two light sources, transmitted light and ultraviolet light. Under the transmitted light, the parameters such as the shape, size and distribution of the inclusions were observed and recorded. Under the ultraviolet light, hydrocarbon and non-hydrocarbon inclusions were classified. The homogenization temperatures of the observed

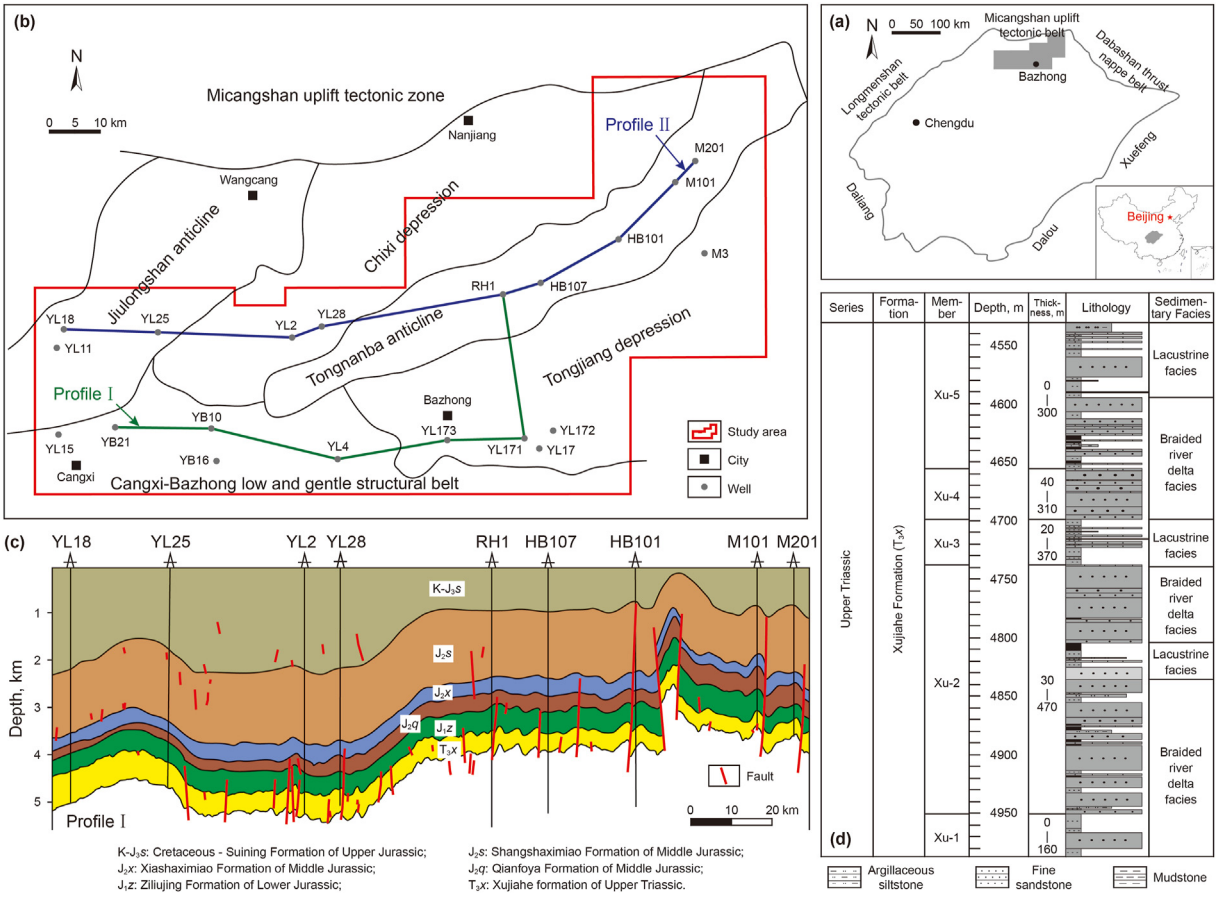


K-J3s: Cretaceous - Suining Formation of Upper Jurassic; J2s: Shangshaximiao Formation of Middle Jurassic;
J2x: Xiashaximiao Formation of Middle Jurassic; J2q: Qianfoya Formation of Middle Jurassic;
J1z: Ziliujing Formation of Lower Jurassic; T3x: Xujiahe formation of Upper Triassic.

**Fig. 1.** Geological characteristics of the study area. (a) Location of northern Sichuan Basin in China. (b) Tectonic units of northern Sichuan Basin. (c) Tectonic profile of northern Sichuan Basin. The location of the profile was presented in (b). (d) Comprehensive stratigraphic histogram of Upper Triassic Xujiahe Formation.

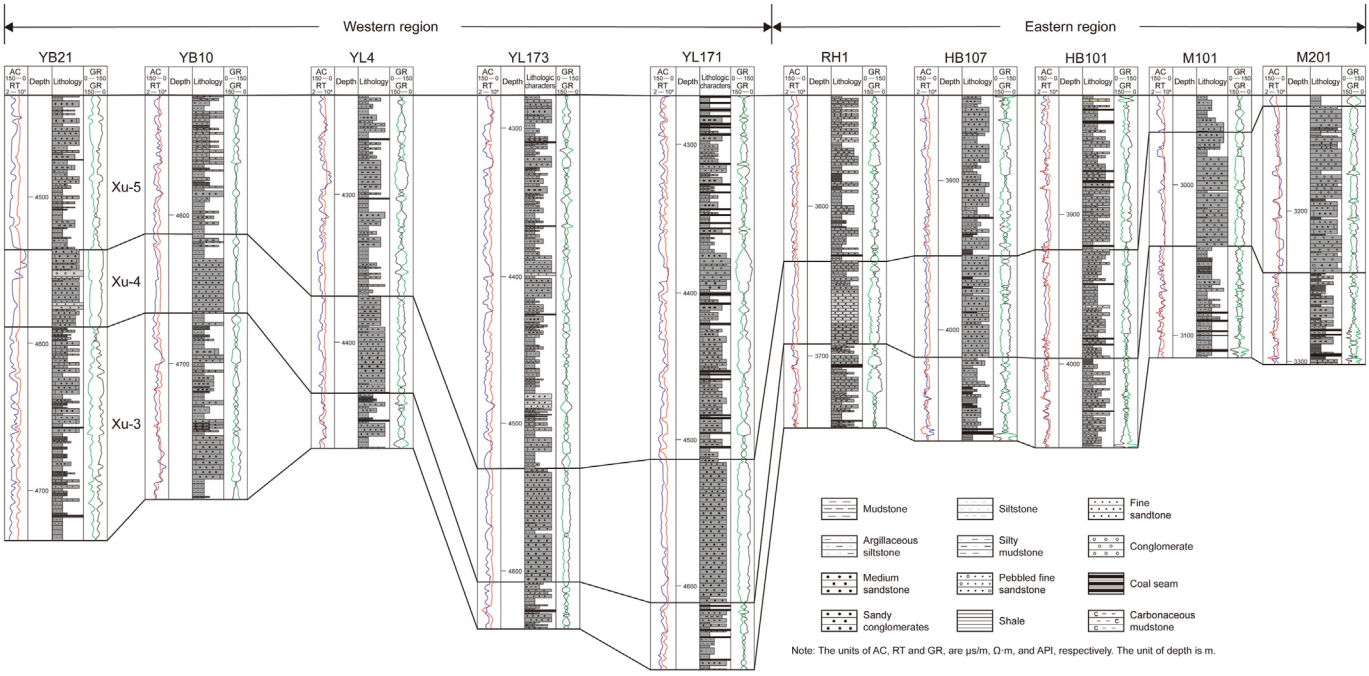


**Fig. 2.** Lateral comparison of source rocks and reservoirs from Xu-3 to Xu-5 members of Xujiahe Formation in northeastern Sichuan Basin. The location of the profile was presented in Figure1(b).

inclusions were measured using a Linkam THMS600 heating and freezing stage. The measurement process was finished by the following steps: raising the temperature to 80 °C at an initial heating rate of 20 °C/min, increasing the temperature to 90 °C at a heating rate of 5 °C/min, raising the temperature at a rate of 1 °C/min to observe the change in inclusion bubbles, increasing the temperature at a rate of 0.1 °C/min when the inclusion bubbles were close to disappear, and recording the homogenization temperature of the inclusion when the bubbles disappear.

The gas-liquid ratio ($F_v$) of hydrocarbon inclusions is one of the important parameters for PVT simulation of fluid inclusions (Aplin et al., 1999). Because gas-hydrocarbon inclusions emitted no or weak fluorescence, it was impossible to measure the gas-liquid ratio of gas-hydrocarbon inclusions by confocal laser scanning microscopy (CLSM). However, based on the CLSM principle (Bourdet et al., 2010), Zhou et al. (2012) proposed a viable method as follows: first, under a high-resolution microscope, the focal length was adjusted according to a certain step to obtain a series of inclusion slices with different step sizes. Then, a graph editing software was used to calculate the areas of inclusions and bubbles in different slices. Finally, fitting the step size–inclusion area and the step size–bubble area polynomial functions, the volume of inclusions and bubbles were obtained by integrating the function, and the volume ratio of bubbles to inclusions was the gas-liquid ratio of inclusions.

### 3.3. Identification of the causes of overpressure

The pressure coefficient (Pc) is the ratio of the formation pressure to the hydrostatic pressure at the same depth, which can reflect whether the formation has developed abnormal pressure. To describe of the formation pressure of Xujiahe Formation in the study area, the division scheme of formation pressure proposed by Hao (2005) was adopted, which divided the pressure into six types: strong negative pressure (Pc < 0.8), negative pressure (0.8 < Pc < 0.96), normal pressure (0.96 < Pc < 1.06), weak overpressure (1.06 < Pc < 1.27), overpressure (1.27 < Pc < 1.73) and strong overpressure (Pc > 1.73).

Acoustic time difference, resistivity and vertical effective stress of mudstone layer were selected as identification parameters to analyze the causes of overpressure. If the abnormally high pressure resulted from fluid expansion, the logging parameters reflected an increase in acoustic time difference and resistivity, and a decrease in the vertical effective stress. If the abnormally high pressure resulted from the tectonic compression, the logging parameters reflected a decrease in the acoustic time difference and vertical effective stress, but an increase in resistivity (Bowers, 2002; Zhao et al., 2017; Liu and Liu, 2018). In the above method, the vertical effective stress was calculated using the following formula:

$$\delta = S - P_p \tag{1}$$

where $\delta$ is the vertical effective stress, MPa; $S$ is the overlying formation pressure, MPa; $P_p$ is the formation pore fluid pressure, MPa.

The overlying formation pressure ($S$) was calculated using the following formula (Shi et al., 2020).

$$S = 0.00980665 \times \left( \rho \times H_0 + \int_{H_0}^{H} \rho_b \mathrm{d}H \right) \tag{2}$$

where $\rho$ and $\rho_b$ are the average density and actual density of overlying formation, respectively, based on logging density data, g/cm$^3$; $H_0$ and $H$ are the initial depth and final depth of a depth segment, respectively, m.

The formation pore fluid pressure ($P_p$) was calculated using the following formula (Eaton, 1975).

$$P_p = S - (S - P_h) \times \left( \frac{\Delta t_n}{\Delta t} \right)^c \tag{3}$$

where $S$ is the overlying formation pressure, MPa; $P_h$ is the hydrostatic pressure, MPa; $\Delta t_n$ is the acoustic time difference of the normal compaction trend line at the same depth, μs/m; $\Delta t$ is the measured acoustic time difference, μs/m; $c$ is the Eaton exponent, with a value of 3.

### 3.4. Research method of natural gas charging period

The natural gas charging periods were determined by the source rock hydrocarbon generation history method and the fluid inclusion method. Of these two methods, the source rock hydrocarbon generation history method restored the burial thermal evolution of a single well through Petromod software, to obtain the geological time corresponding to the main hydrocarbon generation stage, namely, the earliest time for natural gas charging. After observation of fluid inclusions, the homogenization temperature tests and data statistics were conducted for the brine inclusions associated with hydrocarbon inclusions. By mapping the main temperature interval to the burial thermal evolution curve, the corresponding geological time was the natural gas charging time.

### 3.5. Paleo-pressure recovery of reservoir

Restoration of paleo-pressure of Xu-4 member reservoir in the study area were done using a method of combining fluid inclusion PVT simulation (Karlsen et al., 1993; Aplin et al., 1999; Wang et al., 2021) and basin simulation (Wang et al., 2021). The parameters used to carry out PVT simulation of fluid inclusions mainly included homogenization temperature, composition and gas-liquid ratio of the inclusions. The homogenization temperature and gas-liquid ratio of the inclusions were obtained from 3.2. As the inclusion components could not be measured using laser Raman spectroscopy, the natural gas components in current gas reservoirs were used instead. In which, alkane components mainly included $CH_4$, $C_2H_6$, $C_3H_8$, $iC_4$, $nC_4$, $iC_5$ and $nC_5$, nonhydrocarbons components mainly included $CO_2$, $N_2$ and $H_2$, which is basically consistent with the components proposed by Wu et al. (2015, 2019). After obtaining the above parameters, the Sovae-Redlich-Kwong equation of state was used in the PVTsim software for iterative calculation to make the gas-liquid ratio of the set components consistent with the measured gas-liquid ratio (Aplin et al., 1999), then the phase evolution of inclusions was simulated and the trapping pressure (Pt) was obtained, which was equivalent to the paleo-pressure when the inclusion was trapped.

2D basin simulation was conducted using a Petromod software. Basic data, including stratification, sedimentation and uplift time, formation thickness, denudation thickness, lithologic percentage, paleo-thermal flow, paleo water depth, paleo surface temperature, were loaded into the software, the reservoir diagenetic history was constrained by the restored porosity evolution history, and the measured formation pressure and fluid inclusion paleo-pressure were used to restrict the pressure evolution of basin simulation, thereby obtaining the paleo-pressure evolution of the reservoir.

### 3.6. Paleo-pressure recovery of source rock

According to the identification of the causes of overpressure, hydrocarbon generation and tectonic compression were the causes of overpressure in the study area. To restore the paleo-pressure of

Xu-3 member and Xu-5 member, the pressure increase resulted from hydrocarbon generation and tectonic compression were calculated respectively, and the sum of the two was the residual paleo-pressure of the source rocks.

#### 3.6.1. Calculation of the pressure increase resulted from hydrocarbon generation

The amount of pressure increase resulted from the hydrocarbon generation in the source rock was controlled by type, abundance and maturity of the organic matter, as well as the formation sealing conditions (Osborne and Swarbrick, 1997). The quantitative model for calculating the amount of pressure increase of type III kerogen hydrocarbon generation (Eq. (4)) proposed by Guo et al. (2016) was adopted. The theoretical assumptions of this method were as follows: first, under normal compaction, the pores of source rock before hydrocarbon generation were completely filled with formation water. Then, when a certain volume of natural gas ($V_g$) and oil ($V_o$) begin to generate, the sum of the two volumes was equal to the sum of the reduced volume of kerogen ($\Delta V_D$) and the compressed volumes of kerogen ($\Delta V_k$) and pore water ($\Delta V_w$). When the mass of natural gas and oil was obtained, the formation pressure was calculated using the principle of mass conservation. This formation pressure subtracted by the hydrostatic pressure ($P_h$) at this time was the amount of pressure increase resulted from hydrocarbon generation ($P$). Using Eq. (4), the amount of pressure increase resulted from hydrocarbon generation was calculated. The parameters mentioned from Eq. (4) to Eq. (10) were different in different periods, which were obtained through the simulation of the hydrocarbon generation history of the source rocks.

$$P = \frac{B + \sqrt{B^2 + 4AC}}{2A} - P_h \tag{4}$$

where $P$ is hydrocarbon generation pressure, MPa; $P_h$ is the hydrostatic pressure, MPa; $A$ is on behalf of the volume of compression of different substances per unit pressure, $cm^3 \cdot MPa^{-1}$; $B$ is a comprehensive parameter, reflecting the volume of compression of different substances, $cm^3$; $C$ is a parameter related to formation temperature and natural gas volume after the hydracrabon generation.

$P_h$, $A$, $B$ and $C$ in Eq. (4) were calculated as follows:

$$P_h = \rho_w g h \tag{5}$$

$$A = C_w V_{wl} + \frac{1 - IFC_w M_{kl}}{\rho_w} + C_o M_o \Big/ \rho_o \tag{6}$$

$$B = C_w V_{wl} P_h + \frac{1 - IFC_w M_{kl} P_h}{\rho_k} + \frac{7.416 \times 10^{-5} a M_{gr} T_D}{\rho_g} - (M_o + M_g) \Big/ \rho_k + M_o \Big/ \rho_o \tag{7}$$

$$C = 3.413 \times 10^{-4} b M_{gr} T_D \Big/ \rho_g \tag{8}$$

where $\rho_w$ is the average density of formation water, which was 1013 $kg/m^3$; $g$ is the gravitational constant, $m \cdot s^{-2}$; $h$ is the burial depth, m; $C_w$ is the compressibility of water, $0.44 \times 10^{-3}$ $MPa^{-1}$ (Amyx et al., 1960); $V_{wl}$ is the pore water volume, $cm^3$; $I$ is the hydrogen index (HI), $mg \cdot g^{-1}$; $F$ is the conversion rate of kerogen; $C_k$ is the compression coefficient of kerogen, $1.410^{-3}$ $MPa^{-1}$ (Dubow, 1984); $M_{kl}$ is the mass of kerogen, g; $\rho_k$ is the density of kerogen, 1550 $kg/m^3$ (Dubow, 1984); $C_o$ is the oil compression coefficient, $2.2 \times 10^{-3}$ $MPa^{-1}$ (McCain, 1990); $M_o$ is the mass of petroleum, g; $\rho_o$ is petroleum density, 900 $kg/m^3$ (McCain, 1990); $M_{gr}$ is the mass of natural gas remaining in the pores, g; $T_D$ is the formation temperature after hydrocarbon generation, K; $\rho_g$ is the density of natural gas, $kg/m^3$; $M_g$ was the mass of gas, g; $a$ and $b$ are the parameters used to calculate the gas compression factor, the specific obtaining process of that were given in Guo et al. (2016) for the specific obtaining process, please see Eqs. (9) and (10).

$$a = 0.0218(T_D/T_c)^2 - \frac{0.1245 T_D}{T_c} + 0.2091 \tag{9}$$

$$b = -0.2315(T_D/T_c)^2 + \frac{1.333 T_D}{T_c} - 1.0634 \tag{10}$$

where $T_C$ is the formation temperatures when hydrocarbon generation, 190.4 K; $T_D$ is the formation temperature after hydrocarbon generation, K.

The above parameters using in the Eqs. (4)-(10) were presented in Table 1.

#### 3.6.2. Calculation of the pressure increase resulted from tectonic compression

Under closed formation conditions, lateral tectonic compression was one of the important mechanisms leading to formation pressure increase (Luo et al., 2007; Tingay et al., 2009; So and Yuen, 2015), and its mechanism was similar to that of vertical undercompaction (Luo et al., 2007). Based on the mechanism of tectonic compression, Wang et al. (2005) and Zhang et al. (2011) believed that the pressure increase resulted from tectonic compression was as follows:

$$\Delta P = \xi(\sigma_1 - S) \tag{11}$$

where $\Delta P$ was the amount of pressure increase resulted from tectonic compression in MPa; $\xi$ was the sealing coefficient of fluid system, $\xi = 0$–1, where "0″ indicated that the fluid system was completely open, and "1″ suggested that the fluid system was completely closed; $\sigma_1$ was the maximum horizontal principal stress in MPa; $S$ was the overlying formation pressure before tectonic compression in MPa.

The maximum horizontal principal stresses between the west and east of the study area were different in the middle of Yanshan period ($J_3$-early $K_1$) and late Yanshan period ($K_2$). However, judging from the tectonic style, the difference of tectonic stress in the western part is not obvious, and so is that in the eastern part. The calculation of the tectonic stress during $J_3$-early $K_1$ in west and east of the study area was based on the different ratios of tectonic stress during different periods and in different areas from previous researches. According to the calculations of acoustic emission experiments presented by Li et al. (2012), the tectonic compressive stress of the Xujiahe Formation in the study area reached its maximum in the late Yanshan period, and the maximum horizontal principal stresses in the west and east were 169.9 MPa and 144.8 MPa, respectively. According to the research of Cao (2010), the maximum horizontal principal stresses of Xujiahe Formation in Western Sichuan Basin were 76.936 MPa and 107.926 MPa in the middle and late Yanshanian periods, respectively, with the ratio of 1:1.4. Because the maximum horizontal principal stresses of Xujiahe Formation in the middle and late Yanshanian periods had similar ration, the maximum horizontal principal stresses in the west and east of the study area in the middle of Yanshan period were calculated according to the maximum horizontal principal stresses in the late Yanshanian period.

After obtaining the maximum horizontal principal stresses, the

**Table 1**
Parameters of source rocks in the Xu-3 and Xu-5 members during the natural gas charging periods in the study area.

| Area | Well | Member | Time (Ma) | Parameters | | | | | | | | |
|---|---|---|---|---|---|---|---|---|---|---|---|---|
| | | | | $P_h$ (MPa) | $V_{wl}$ (cm$^3$) | $I$ (mg/g) | $F$ (%) | $M_{kl}$ (g) | $M_o$ (g) | $M_{gr}$ (g) | $M_g$ (g) | $T_D$ (K) |
| Western region | YB16 | $T_3x^5$ | 160 | 28.6 | 45297.9 | 125 | 6.3 | 28530.7 | 65.3 | 141.7 | 141.8 | 379.5 |
| | | | 140 | 43.7 | 30520.3 | 125 | 65.7 | 28530.7 | 165.3 | 434.5 | 434.6 | 425.3 |
| | | $T_3x^3$ | 160 | 29.1 | 44493.7 | 125 | 8.7 | 18048.5 | 55.9 | 120.2 | 120.3 | 381.2 |
| | | | 140 | 44.3 | 30165.8 | 125 | 69.2 | 18048.5 | 33.0 | 77.9 | 78.0 | 427.0 |
| | YL2 | $T_3x^5$ | 160 | 28.7 | 45083.5 | 125 | 8.3 | 5739.2 | 16.7 | 37.0 | 37.1 | 380.0 |
| | | | 140 | 45.2 | 29615.5 | 125 | 70.6 | 5739.2 | 24.9 | 80.8 | 80.9 | 429.6 |
| | | $T_3x^3$ | 160 | 29.3 | 44273.1 | 125 | 10.4 | 29958.8 | 107.8 | 235.7 | 235.8 | 376.7 |
| | | | 140 | 45.7 | 29275.7 | 125 | 72.4 | 29958.8 | 120.3 | 411.5 | 411.6 | 431.3 |
| | YL4 | $T_3x^5$ | 160 | 28.1 | 46027.6 | 125 | 6.0 | 8425.4 | 40.6 | 40.5 | 40.6 | 378.0 |
| | | | 140 | 43.3 | 30836.5 | 125 | 66.1 | 8425.4 | 97.7 | 138.9 | 139.0 | 423.9 |
| | | $T_3x^3$ | 160 | 28.8 | 45026.6 | 125 | 8.1 | 24914.2 | 70.3 | 159.4 | 159.5 | 380.1 |
| | | | 140 | 43.9 | 30403.4 | 125 | 69.2 | 24914.2 | 92.4 | 373.7 | 373.8 | 425.9 |
| | YL11 | $T_3x^5$ | 160 | 23.3 | 54406.7 | 125 | 2.1 | 11432.9 | 0 | 28.6 | 28.8 | 363.7 |
| | | | 140 | 39.4 | 33655.2 | 125 | 53.7 | 11432.9 | 93.3 | 209.9 | 210.0 | 412.3 |
| | | $T_3x^3$ | 160 | 24.0 | 53112.2 | 125 | 3.4 | 5265.3 | 6.7 | 14.9 | 15.0 | 365.6 |
| | | | 140 | 40.0 | 33201.6 | 125 | 57.8 | 5265.3 | 41.1 | 94.4 | 94.5 | 414.0 |
| | YL15 | $T_3x^5$ | 160 | 24.9 | 51300.3 | 125 | 1.9 | 3337.7 | 2.6 | 5.1 | 5.2 | 368.5 |
| | | | 140 | 41.1 | 32388.6 | 125 | 54.3 | 3337.7 | 26.6 | 59.3 | 59.3 | 417.2 |
| | | $T_3x^3$ | 160 | 25.9 | 49539.1 | 125 | 3.6 | 8188.5 | 10.8 | 24.4 | 24.5 | 371.4 |
| | | | 140 | 42.0 | 31712.7 | 125 | 59.2 | 8188.5 | 58.2 | 140.4 | 140.5 | 420.1 |
| | YL17 | $T_3x^5$ | 160 | 30.1 | 43202.0 | 125 | 5.7 | 11243.5 | 22.9 | 51.2 | 51.3 | 384.1 |
| | | | 140 | 45.5 | 29432.5 | 125 | 6.1 | 11243.5 | 83.1 | 182.5 | 182.6 | 430.5 |
| | | $T_3x^3$ | 160 | 31.4 | 41616.2 | 125 | 9.0 | 22330.4 | 69.3 | 155.6 | 155.7 | 387.9 |
| | | | 140 | 46.6 | 28728.1 | 125 | 66.9 | 22330.4 | 149.9 | 330.3 | 330.4 | 434.1 |
| | YL28 | $T_3x^5$ | 160 | 28.9 | 44871.1 | 125 | 11.0 | 5404.0 | 20.3 | 44.5 | 44.6 | 380.4 |
| | | | 140 | 44.0 | 30377.5 | 125 | 68.6 | 5404.0 | 29.5 | 80.7 | 80.8 | 426.0 |
| | | $T_3x^3$ | 160 | 29.6 | 43848.8 | 125 | 13.8 | 9460.9 | 43.4 | 95.0 | 95.1 | 382.6 |
| | | | 140 | 44.6 | 29938.3 | 125 | 70.8 | 9460.9 | 38.2 | 148.5 | 148.6 | 428.1 |
| | YL172 | $T_3x^5$ | 160 | 29.7 | 43731.0 | 125 | 12.8 | 11686.1 | 0 | 109.8 | 109.9 | 382.9 |
| | | | 140 | 45.5 | 29378 | 125 | 75.2 | 11686.1 | 3.5 | 29.3 | 29.3 | 430.8 |
| | | $T_3x^3$ | 160 | 31.1 | 41909.3 | 125 | 18.5 | 5299.6 | 18.4 | 49.9 | 50.0 | 387.2 |
| | | | 140 | 46.9 | 28590.2 | 125 | 78.6 | 5299.6 | 0.2 | 4.9 | 4.9 | 434.8 |
| | YL173 | $T_3x^5$ | 160 | 29.1 | 44604.9 | 125 | 9.8 | 9456.3 | 31.7 | 70.7 | 70.8 | 381.0 |
| | | | 140 | 45.2 | 29597.1 | 125 | 73.1 | 9456.3 | 23.1 | 123.1 | 123.2 | 429.7 |
| | | $T_3x^3$ | 160 | 29.9 | 43451.7 | 125 | 14.9 | 33490.3 | 163.0 | 356.9 | 357.0 | 383.5 |
| | | | 140 | 46.0 | 29120.5 | 125 | 76.7 | 33490.3 | 60.5 | 378.1 | 378.2 | 432.1 |
| Eastern region | M3 | $T_3x^5$ | 160 | 30.3 | 42968.1 | 125 | 8.0 | 15040.5 | 43.2 | 94.9 | 95.0 | 384.7 |
| | | | 140 | 48.1 | 27919.6 | 125 | 71.6 | 15040.5 | 77.5 | 247.9 | 248.0 | 438.4 |
| | | $T_3x^3$ | 160 | 31.0 | 41995.5 | 125 | 12.3 | 7586.4 | 31.6 | 69.7 | 69.8 | 387.0 |
| | | | 140 | 48.8 | 27516.3 | 125 | 74.9 | 7586.4 | 28.5 | 131.8 | 131.8 | 440.7 |
| | M201 | $T_3x^5$ | 160 | 23.8 | 53470 | 125 | 6.6 | 10303.2 | 26.2 | 52.2 | 52.3 | 365.1 |
| | | | 140 | 35.5 | 37137.3 | 125 | 73.6 | 10303.2 | 33.5 | 143.8 | 143.9 | 400.3 |
| | | $T_3x^3$ | 160 | 25.0 | 51080.2 | 125 | 10.0 | 27741.0 | 95.6 | 212.2 | 212.4 | 368.8 |
| | | | 140 | 36.6 | 36050.2 | 125 | 76.7 | 27741.0 | 40.5 | 235.2 | 235.3 | 403.8 |

amounts of pressure increase resulting from tectonic compression in the west and east of the study area in the middle Yanshanian periods were calculated according to Eq. (11). In the process of calculating the pressure of the overlying formation, the paleo burial depths of Xu-3 member and Xu-5 member were obtained using the basin simulation method, with the density of the formation taking the value of 2000 kg/m$^3$.

## 4. Results

### 4.1. Current formation pressure characteristics and the causes of overpressure

By statistical analysis, the formation pressure of Xujiahe Formation in northeastern Sichuan Basin ranged from 36.4 MPa to 106.5 MPa, the pressure coefficients mainly ranged from 1.01 to 2.22 (Fig. 3), which were classified as normal pressure and strong overpressure. Among the members, the formation pressure of Xu-4 member ranged from 37.0 to 93.6 MPa, and the pressure coefficient ranged from 1.04 to 2.22, which were also belonged to normal pressure or strong overpressure. The present formation pressures of Xujiahe Formation in the west and east of the study area were different. The formation pressures in the western region ranged from 34.6 to 106.5 MPa (Fig. 3a), and their pressure coefficients ranged from 0.99 to 2.22 (Fig. 3b), while the formation pressures in the eastern region ranged from 39.1 to 100.9 MPa (Fig. 3c), and their pressure coefficients ranged from 1.2 to 2.0 (Fig. 3d). Therefore, the formation pressure in the western region was slightly greater than that in the eastern region. For the Xu-4 member, the formation pressures in the western region ranged from 36.5 to 91.8 MPa (Fig. 3a), and their pressure coefficients ranged from 1.19 to 2.16 (Fig. 3b). The formation pressures in the eastern region ranged from 49.9 to 90.2 MPa (Fig. 3c), and the pressure coefficients ranged from 1.24 to 1.86 (Fig. 3d). So the formation pressure of the Xu-4 member in the western region was also slightly greater than that in the eastern region.

By the log responses of fluid pressure (Fig. 4) of well YB16 and Well M201 in northern Sichuan Basin, it was revealed that the acoustic travel time of Xu-3, Xu-4 and Xu-5 has three trends: no change, a small amount of increase or a small amount of decrease, the resistivity tends to increase or not to change, and the density is mainly constant, indicating that the overpressure is complex, and mainly caused by tectonic compression and fluid expansion. According to the relationship diagrams of vertical effective stress -

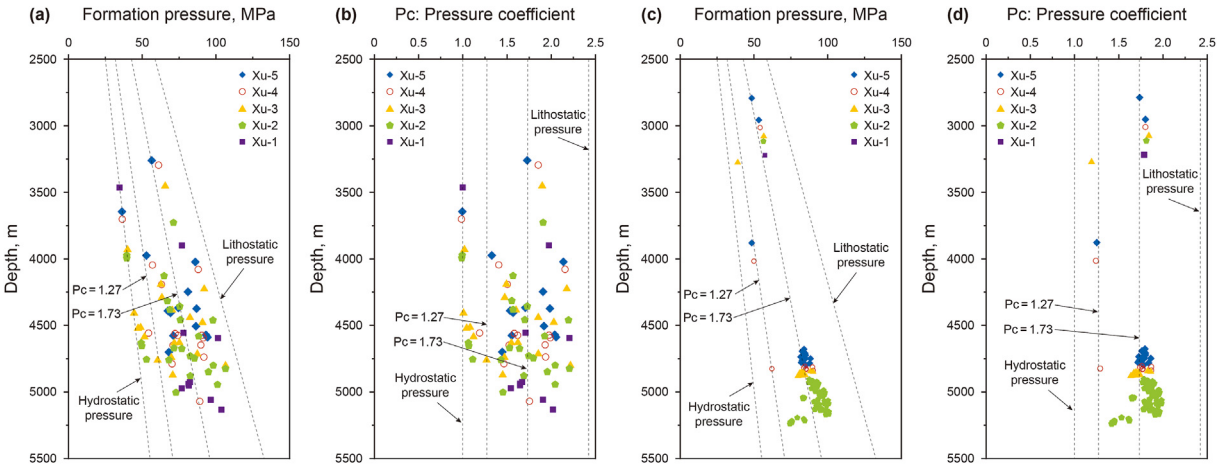


**Fig. 3.** Vertical distributions of current formation pressures and pressure coefficients (Pc) in different members of Xujiahe Formation in northeastern Sichuan Basin. (a), (b) present the western region, and (c), (d) present the eastern region.

acoustic travel time (Fig. 5a), density - acoustic travel time (Fig. 5b) and vertical effective stress - density (Fig. 5c) of formations with normal and abnormal pressures, it was shown that acoustic travel time, vertical effective stress and density of Xu-3, Xu-4 and Xu-5 members with overpressure deviated from normal compaction trend line, which mainly exhibited in two cases: (1) the increase of acoustic travel time, the decrease of vertical effective stress and the slight decrease of density reflected that the overpressure was caused by fluid expansion; (2) the decrease of acoustic travel time, the increase of density and the non-obvious change of vertical effective stress together indicated that the overpressure was caused by tectonic compression. Meanwhile some data points are between fluid expansion and tectonic compression, and there is no obvious difference between the causes of overpressure in western and eastern regions. It should be noted that the overpressure and overpressure origin described here is the final state after the formation and transformation of overpressure.

From the relationship between formation overpressure and TOC of source rocks from Upper Triassic to Jurassic in western area of northeastern Sichuan Basin (Fig. 6), it was found that the pressure coefficient was positively correlated with TOC, and the degree of overpressure was increased with the increase of organic matter abundance of source rocks, revealing that hydrocarbon generation of source rocks was the main factor leading to overpressure caused by fluid expansion. For the eastern area, the tectonic compression overpressure is caused by the multi-stage tectonic activities in the study area.

### 4.2. Formation burial history and hydrocarbon generation history

The basin simulation results (Fig. 7) indicated that the Xujiahe Formation in the study area began to deposit in the Late Triassic ($T_3$). The deposition rate of the formation in the western region was slightly higher than that in the eastern region in the Late Jurassic ($J_3$), but that in the western region was significantly lower than that in the eastern region in the Early Cretaceous ($K_1$). The maximum burial depth of about 6000 m was reached at the end of $K_1$. Since the Late Cretaceous ($K_2$), tectonic uplift has occurred in the western and eastern regions, resulting in intense erosion of the overlying formation.

According to the simulation results of hydrocarbon generation, the maturity of source rocks of Xujiahe Formation in the study area increased during the burial process, and was inhibited by the decrease of formation temperature during the uplift process. The values of vitrinite reflectance ($R_o$) of Xujiahe Formation source rocks in the whole area reached 0.7%–1.0% in the $J_3$, which entered into the mature stage. The $R_o$ values reached 1.3% in the $K_1$, and some of them even reached over 2.0%, entering into the high or over mature stages. Due to the difference in burial history and heat flow, the maturity of source rocks in the western region was lower than that in the eastern region in the $K_1$. Only a small part of the source rocks in the western region had $R_o$ values over 2.0%, while that in the eastern region all exceeded 2.0%. Since the $K_2$, the maturity of source rocks has almost no increase due to the tectonic uplift.

### 4.3. Characteristics of fluid inclusions in the reservoir

According to the observation under transmitted light and fluorescent light, gas hydrocarbon inclusions, brine inclusions and a small amount of asphalt inclusions were developed in Xu-4 member reservoir of Xujiahe Formation in the study area. Among these inclusions, the gas hydrocarbon inclusions and their associated brine inclusions were mostly in the form of beads or clusters distributed in the healing cracks of quartz particles (Fig. 8a), and a small amount were distributed in the secondary enlarged sides of quartz particles. The sizes of the inclusions were mainly ranged from 5 to 15 μm. The inside of gas hydrocarbon inclusions had a homogeneous gas phase, and their associated brine inclusions were mostly of vapor-liquid phases, in which bubbles occupied 10%–20% of the apparent area of the inclusions. Most of the gas hydrocarbon inclusions and their associated brine inclusions were not shown under fluorescence, and a few gas hydrocarbon inclusions emitted weak white fluorescence (Fig. 8b). The asphalt-containing inclusions were small in size (Fig. 8c), partially destroyed with irregular shape, which performed black under transmitted light and white under fluorescence (Fig. 8d).

The homogenization temperatures of the brine inclusions associated with gas hydrocarbon inclusions in the Xu-4 member reservoir of Xujiahe Formation ranged from 92.1 to 164.4 °C, and the gas-liquid ratios of that ranged from 7.3% to 15.2%. For the gas compositions of bubbles of brine inclusions, the $CH_4$ content was the highest, ranging from 0.121% to 0.644%. The content of different hydrocarbon compositions gradually decreased with the increase of their molecular weights, and the $C_5H_{12}$ content was the lowest, ranging from 0.000013% to 0.000066%. In terms of the compositions of inorganic gas, the $H_2$ contents ranged from 0.00007% to 0.00119%, $N_2$ contents ranged from 0.001% to 0.009%, and $CO_2$ contents ranged from 0.00051% to 0.00423% (Table 2).

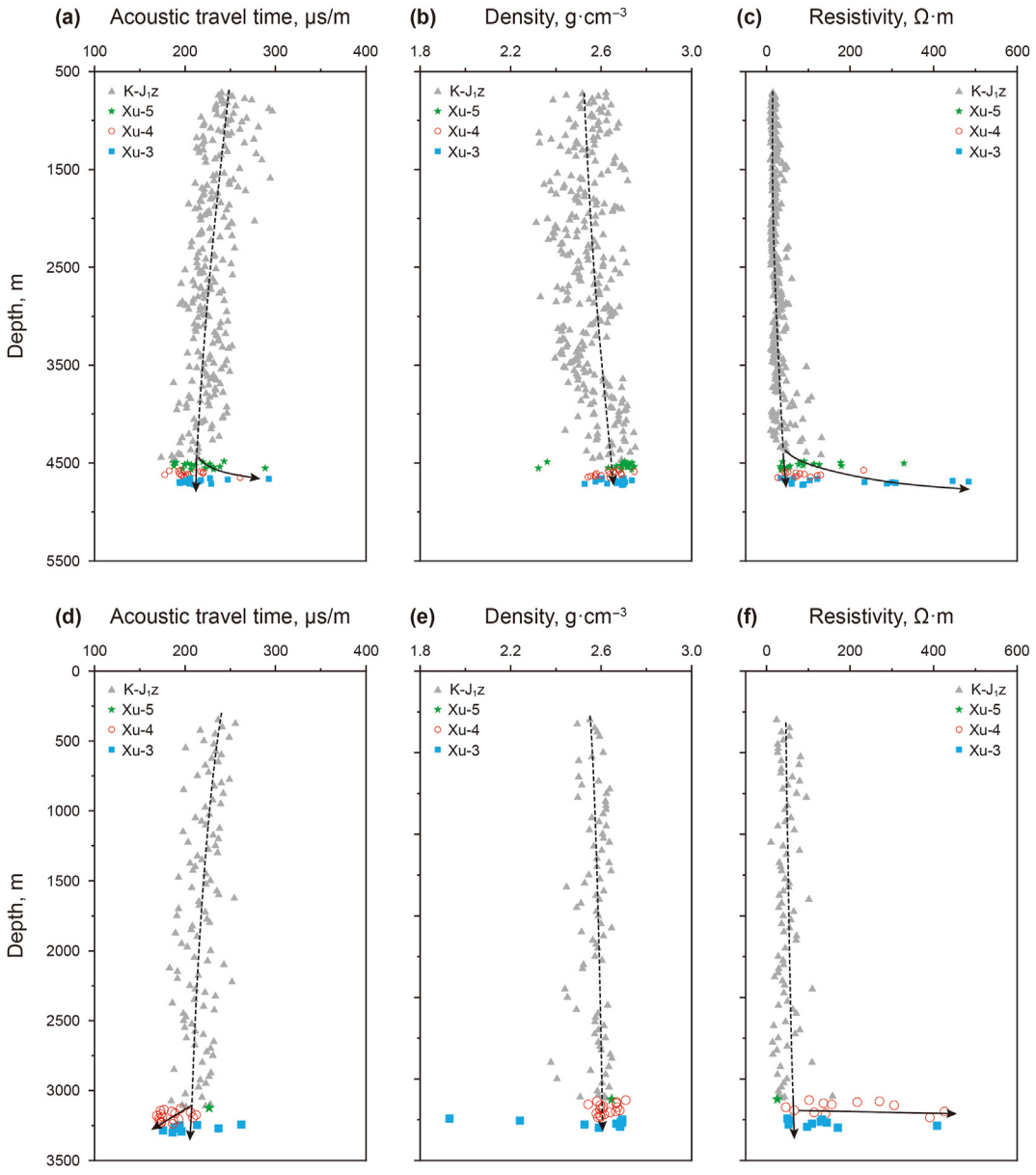


**Fig. 4.** Log responses of fluid pressure for Well YB16 (a–c) and Well M201 (d–f) in northern Sichuan Basin.

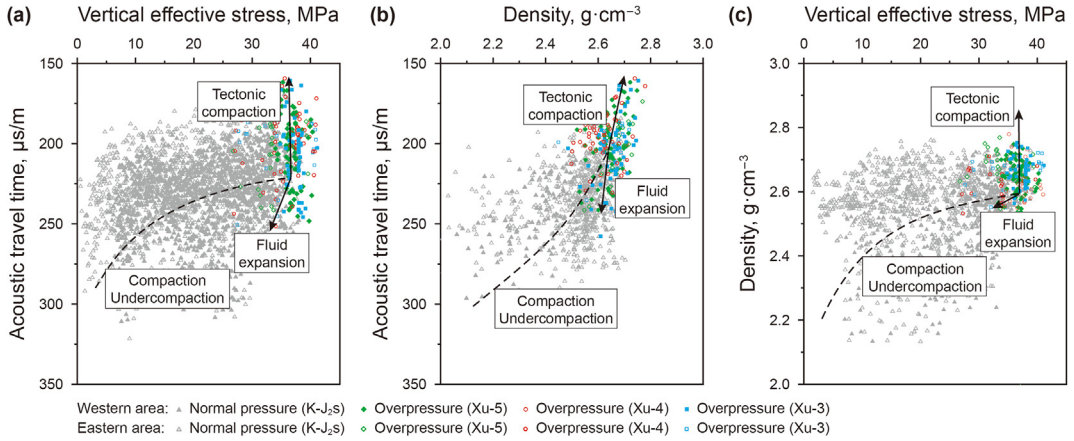


**Fig. 5.** Identification of different causes of overpressure using logging data in northern Sichuan Basin (The identification templates were from Zhao et al., modified). (a) Relationship between vertical effective stress and acoustic travel time. (b) Relationship between density and acoustic travel time. (c) Relationship between vertical effective stress and density.

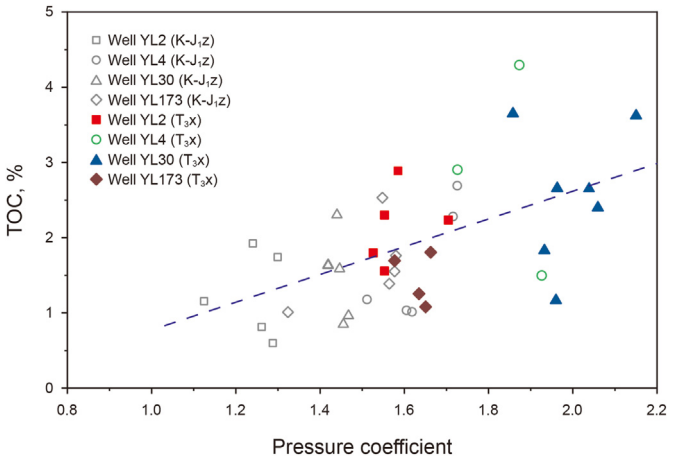


**Fig. 6.** Relationship between formation pressure coefficient and total organic carbon (TOC) of source rocks with overpressure in northern Sichuan Basin. The pressure coefficient was positively correlated with TOC, revealing that hydrocarbon generation was the main cause for fluid expansion.

### 4.4. Natural gas charging period

Previous research (Li et al., 2012) shown that the natural gas would be generated when the $R_o$ value of Xujiahe Formation source rocks in northeastern Sichuan Basin reached 0.6%, and a large amount of natural gas would be generated when $R_o$ value reached over 0.7%, and the peak value of natural gas generation appeared when $R_o$ value was 1.0%. According to this evaluation standards, the source rocks of Xujiahe Formation in the study area began to generate natural gas in the Middle Jurassic ($J_2$), began to generate a large amount of natural gas in the early $J_3$, reached the peak of natural gas generation in the late $J_3$, and reached the over mature stage in the $K_1$.

In the Xu-4 member reservoir of the Xujiahe Formation in the study area, the homogenization temperatures of brine inclusions associated with hydrocarbon inclusions were mainly distributed over the range of 80–180 °C. In contrast, the two homogenization temperature peaks of brine inclusions in the western region were 90–100 °C and 130–170 °C, and that in the eastern region were 90–120 °C and 130–170 °C. Combined with the thermal evolution history, it was considered that the main natural gas charging periods of Xu-4 member reservoir of the Xujiahe Formation were the $J_2$, the $J_3$ – the early $K_1$, and there was only a small difference in natural gas charging periods between the western and eastern regions.

### 4.5. Pressure evolution of the reservoir

Based on the parameters such as homogenization temperature, composition and gas-liquid ratio of fluid inclusions, the paleo-pressures of Xu-4 member reservoir of Xujiahe Formation, simulated by PVTsim software. It shown that the paleo-pressures from $J_2$ to $K_1$ exhibited a gradually increasing trend, with a range from 12.7 to 89.6 MPa and a pressure coefficients of 0.98–1.79 (Table 3).

Taking the above present pressures and paleo-pressures as correction values, the pressure evolution history was simulated using the basin simulation method. The pressure evolution history of Xu-4 member reservoir of Xujiahe Formation was shown in Fig. 9. It was observed that the residual pressures ranged from 8 to 12 MPa at the end of $J_2$ deposition, from 22 to 33 MPa at the end of $J_3$ deposition, and from 20 to 27 MPa at the end of $K_1$ deposition. Tectonic uplifting in the end of $J_3$ and form $K_2$ to present is relatively obvious for pressure release. The residual pressures after the period of $J_2$ in the western region were higher than that in the eastern region, and the pressure in the eastern region decreased relatively rapidly from $K_2$ to present.

### 4.6. Pressure evolution of the source rocks

#### 4.6.1. Amount of hydrocarbon generation pressure

PetroMod software was used to simulate the thermal evolution history of Xu-3 member and Xu-5 member, and the hydrocarbon generation and expulsion parameters during the critical charging periods were obtained. The organic matter conversion rate ($F$) of source rocks at 160 Ma in the $J_2$ ranged from 1.9% to 18.5%, while that ranged from 53.7% to 76.7% at 140 Ma in the $K_1$. By Eq. (4), the amounts of hydrocarbon generation pressure of Xu-3 member and Xu-5 member during the critical charging periods were calculated, as shown in Table 3. The amounts of hydrocarbon generation pressure of Xu-3 member ranged from 3.1 to 27.5 MPa in the $J_2$, from 5.6 to 45.2 MPa in the $J_3$ – the early $K_1$. The amount of hydrocarbon generation pressure increase of Xu-5 member ranged from 1.2 to 15.6 MPa in the $J_2$, from 1.4 to 40.1 MPa in the $J_3$ – the early $K_1$. It can be seen that the amounts of hydrocarbon generation

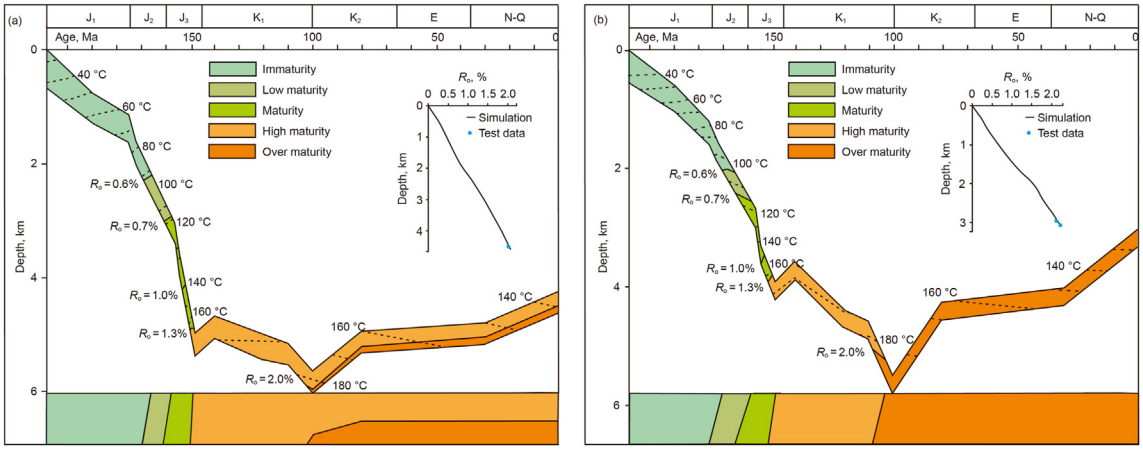


**Fig. 7.** Burial history of Xujiahe Formation and hydrocarbon generation history of source rocks in northern Sichuan Basin. (a) Represents the western region (well YL17), and (b) represents the eastern region (well M201). During $J_2$ and $J_3$, the source rocks of Xujiahe Formation in both western and eastern regions entered into mature stages. During $K_1$, the source rocks in western region entered into high-over mature stage, while all source rocks in eastern region entered into over mature stage.

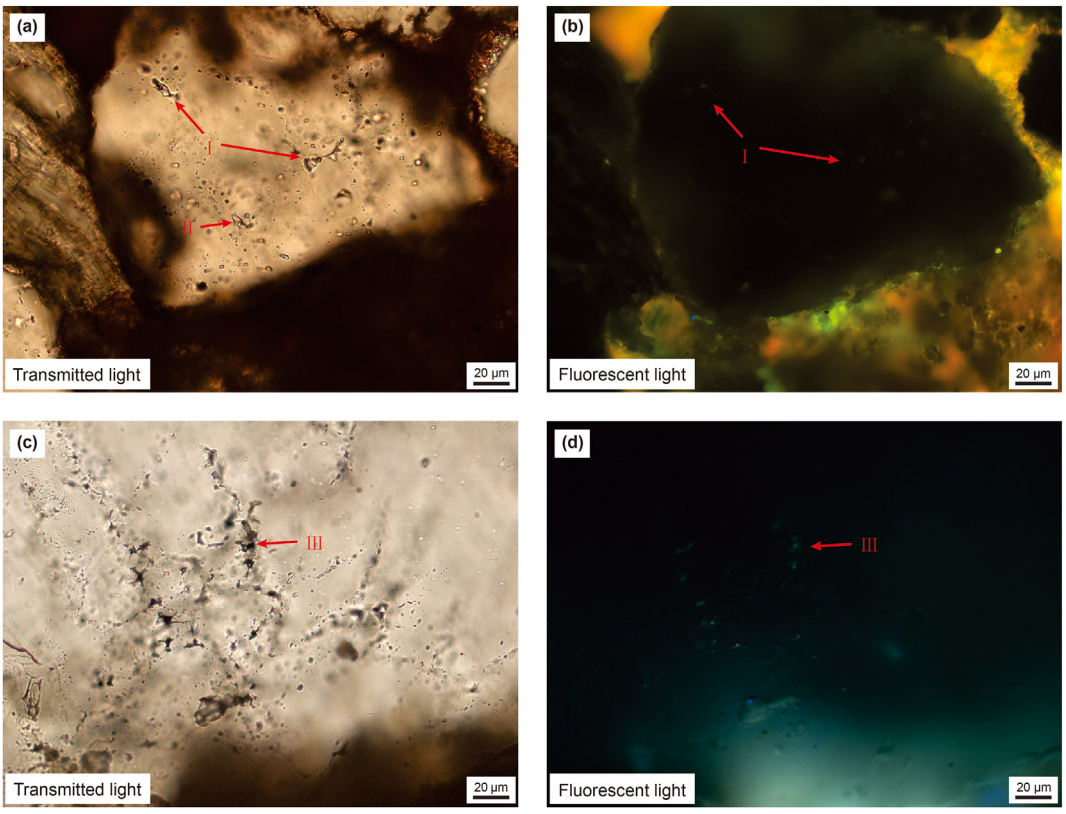


**Fig. 8.** Characteristics of fluid inclusions in the Xu-4 member reservoir in northern Sichuan Basin.
(a) Well YL2, 4912.26 m, gas hydrocarbon inclusions (I) and their associated brine inclusions (II) beaded distribution in the healing fractures of quartz particles, photo under transmitted light; (b) Corresponds to (a), gas hydrocarbon inclusions (I) emitted faint white fluorescence, brine inclusions (II) emitted no light, photo under fluorescent light; (c) YL4, 4458.7 m, black asphalt-containing inclusions (III) with irregular shape, photo under transmitted light; (d) Corresponds to (c), asphalt-containing inclusions (III) with white fluorescence, photo under fluorescent light.

pressure of Xu-3 member were greater than that of Xu-5 member on the whole. But the amounts of hydrocarbon generation pressure of both Xu-3 member and Xu-5 member differed greatly in different wells on the plane. During the $J_2$, the amount of hydrocarbon generation pressure of Xu-3 member ranged from 3.1 to 27.5 MPa in the western region, from 12.6 to 19.1 MPa in the eastern region, and that of Xu-5 member ranged from 1.2 to 15.6 MPa in the western region, from 8.3 to 13.3 MPa in the eastern region. From the $J_3$ – the early $K_1$, the amounts of hydrocarbon generation pressure of Xu-3 member ranged from 5.6 to 20.7 MPa in the western region, from 6.0 to 45.2 MPa in the eastern region, and that of Xu-5 member ranged from 1.4 to 14.2 MPa in the western region, from 1.7 to 40.1 MPa in the eastern region.

#### 4.6.2. Amount of tectonic compression pressure

By Eq. (11), the amounts of tectonic compression pressure of Xu-3 and Xu-5 members of Xujiahe Formation during the critical charging periods of natural gas were shown in Table 3. The amounts of tectonic compression pressure of Xu-3 and Xu-5 members ranged from 6.9 to 40.8 MPa and from 8.3 to 42.7 MPa, respectively. There had differences in the stresses involved in lateral tectonic compression between the western and eastern regions, leading to differences in the amounts of tectonic compression pressure. The amounts of tectonic compression pressure in the western region were larger than that in the eastern region. There were also differences in the amounts of tectonic compression pressure in different tectonic belts. The core of anticline had the largest tectonic compression pressure, such as wells YL18, YL11 in the western region and well M201 in the eastern region, while the depression and low-gentle tectonic zone had relatively little tectonic compression pressure.

#### 4.6.3. Overpressure of the source rock during the critical charging periods

During the $J_2$, the main cause of overpressure in the source rocks of the Xujiahe Formation in the study area was hydrocarbon generation. From the $J_3$ to the $K_1$, the causes of overpressure included hydrocarbon generation and tectonic compression. Based on the calculation of hydrocarbon generation pressure and tectonic compression pressure, the residual pressures of Xu-3 member and Xu-5 member source rocks during the critical charging periods were obtained, as shown in Table 3. The residual pressures of source rocks differed greatly in different members and different wells. The residual pressures of Xu-3 member and Xu-5 member source rocks during the $J_2$ ranged from 3.1 to 27.5 MPa and from 1.2 to 15.6 MPa, respectively, and that during the $J_3$ – the $K_1$ ranged from 36.9 to 52.1 MPa and from 34.9 to 48.4 MPa, respectively. During the $J_2$, the residual pressures ranged from 3.1 to 27.5 MPa in Xu-3 member and from 1.2 to 15.6 MPa in Xu-5 member in the western region, while the residual pressures ranged from 12.6 to 19.1 MPa in Xu-3 member and from 8.3 to 13.3 MPa in Xu-5 member in the eastern region. During the $J_3$ – the $K_1$, the residual pressures in the western region ranged from 43.4 to 49.3 MPa in Xu-3 member and from 38.3 to 46.2 MPa in Xu-5 member, while the residual pressures in the eastern region ranged from 36.9 to 52.1 MPa in Xu-3 member and from 34.9 to 48.4 MPa in Xu-5 member.

**Table 2**
Characteristics and paleo-pressure simulation results of fluid inclusions in the Xu-4 member reservoir in northern Sichuan Basin.

| Well | Depth (m) | Th (°C) | $F_v$ (%) | Molar Percentage (mol %) | | | | | | | | | | Age (Ma) | Period | Paleo-depth (m) | Pt (MPa) | Pc |
|---|---|---|---|---|---|---|---|---|---|---|---|---|---|---|---|---|---|---|
| | | | | $C_1$ | $C_2$ | $C_3$ | $iC_4$ | $nC_4$ | $iC_5$ | $nC_5$ | $H_2$ | $N_2$ | $CO_2$ | | | | | |
| YL17 | 4540 | 92.1 | 7.3 | 0.22 | 0.002 | 0.00082 | 0.00007 | 0.00007 | 0.000023 | 0.000023 | 0.00107 | 0.002 | 0.00223 | 168 | $J_2$ | 2430 | 30.9 | 1.3 |
| YL17 | 4540 | 142 | 12.9 | 0.476 | 0.001 | 0.00006 | 0.00005 | 0.00005 | 0.00048 | 0.000048 | 0.00048 | 0.002 | 0.00261 | 149 | $J_3$–$K_1$ | 4235 | 65.8 | 1.59 |
| YL17 | 4540 | 136 | 11.5 | 0.44 | 0.01 | 0.001 | 0.00009 | 0.00009 | 0.000046 | 0.000046 | 0.00014 | 0.003 | 0.00219 | 151 | $J_3$–$K_1$ | 4080 | 67.8 | 1.7 |
| YL17 | 4540 | 164 | 15.2 | 0.644 | 0.007 | 0.00145 | 0.00013 | 0.00013 | 0.000066 | 0.000066 | 0.0002 | 0.004 | 0.00317 | 129 | $J_3$–$K_1$ | 5110 | 89.6 | 1.79 |
| YL17 | 4540 | 156 | 14.5 | 0.565 | 0.005 | 0.00046 | 0.00006 | 0.00006 | 0.00029 | 0.000029 | 0.00023 | 0.003 | 0.00423 | 143 | $J_3$–$K_1$ | 4766 | 76.7 | 1.64 |
| YL17 | 4540 | 96 | 7.7 | 0.23 | 0.002 | 0.00086 | 0.00007 | 0.00007 | 0.00029 | 0.000029 | 0.00119 | 0.002 | 0.00233 | 166 | $J_2$ | 2545 | 32.2 | 1.29 |
| YL172 | 5137.2 | 111.6 | 9.1 | 0.33 | 0.006 | 0.0007 | 0.00007 | 0.00007 | 0.00034 | 0.000034 | 0.00017 | 0.003 | 0.00140 | 161 | $J_2$ | 3100 | 47.0 | 1.73 |
| YL172 | 5137.2 | 169.5 | 16.0 | 0.67 | 0.015 | 0.0015 | 0.00014 | 0.00014 | 0.00069 | 0.000069 | 0.00021 | 0.004 | 0.00333 | 88 | $K_2$ | 5580 | 87.2 | 1.7 |
| YB16 | 4625.1 | 140.5 | 12.8 | 0.45 | 0.001 | 0.0001 | 0.00004 | 0.00004 | 0.00046 | 0.000046 | 0.00046 | 0.002 | 0.0025 | 152 | $J_3$–$K_1$ | 4063 | 62.5 | 1.6 |
| YB16 | 4625.1 | 159.9 | 15.8 | 0.52 | 0.005 | 0.0004 | 0.00005 | 0.00005 | 0.00027 | 0.000027 | 0.00021 | 0.003 | 0.0004 | 147 | $J_3$–$K_1$ | 4744 | 58.9 | 1.4 |
| YL2 | 4630.3 | 176.4 | 17.8 | 0.68 | 0.008 | 0.0009 | 0.00007 | 0.00007 | 0.00007 | 0.000070 | 0.0008 | 0.009 | 0 | 121 | $J_3$–$K_1$ | 5529 | 75.8 | 1.5 |
| YL4 | 4405.1 | 138.4 | 11.9 | 0.49 | 0.006 | 0.0006 | 0.00005 | 0.00005 | 0.00005 | 0.000050 | 0.0006 | 0.006 | 0 | 130 | $J_3$–$K_1$ | 5170 | 72.5 | 1.5 |
| YL4 | 4405.1 | 149.5 | 20.5 | 0.50 | 0.013 | 0.0018 | 0.00026 | 0.00026 | 0.00052 | 0.000052 | 0.0003 | 0.005 | 0.0005 | 133 | $J_3$–$K_1$ | 5030 | 71.3 | 1.5 |
| YL4 | 4405.1 | 140.6 | 12.3 | 0.50 | 0.001 | 0.0001 | 0.00005 | 0.00005 | 0.00051 | 0.000051 | 0.0005 | 0.002 | 0.0027 | 148 | $J_3$–$K_1$ | 5050 | 70.4 | 1.5 |
| YL11 | 4210.3 | 141.5 | 13.3 | 0.42 | 0.004 | 0.0003 | 0.00004 | 0.00004 | 0.00021 | 0.000021 | 0.0002 | 0.002 | 0.0031 | 145 | $J_3$–$K_1$ | 4230 | 50.1 | 1.2 |
| YL15 | 4138.2 | 152.9 | 14.6 | 0.50 | 0.005 | 0.0004 | 0.00005 | 0.00005 | 0.00026 | 0.000026 | 0.0002 | 0.003 | 0.004 | 138 | $J_3$–$K_1$ | 4450 | 60.7 | 1.4 |
| YL28 | 4750 | 136.7 | 12.2 | 0.43 | 0.009 | 0.0010 | 0.00009 | 0.00009 | 0.00044 | 0.000044 | 0.0001 | 0.002 | 0.002 | 141 | $J_3$–$K_1$ | 4530 | 58.9 | 1.3 |
| YL28 | 4750 | 127.6 | 10.9 | 0.40 | 0.009 | 0.0009 | 0.00008 | 0.00008 | 0.00042 | 0.000042 | 0.0001 | 0.002 | 0.002 | 142 | $J_3$–$K_1$ | 4350 | 47.9 | 1.1 |
| M201 | 3157 | 120 | 10.7 | 0.301 | 0.006 | 0.00065 | 0.00006 | 0.00006 | 0.00031 | 0.000031 | 0.00016 | 0.003 | 0.00128 | 158 | $J_3$–$K_1$ | 3812 | 41.1 | 1.44 |
| M201 | 3157 | 92.9 | 7.7 | 0.121 | 0.002 | 0.00026 | 0.00003 | 0.00003 | 0.00013 | 0.000013 | 0.00006 | 0.001 | 0.00051 | 175 | $J_2$ | 1591 | 12.7 | 0.99 |
| M201 | 3157 | 96.1 | 8.1 | 0.138 | 0.002 | 0.0003 | 0.00003 | 0.00003 | 0.00014 | 0.000014 | 0.00007 | 0.001 | 0.00058 | 174 | $J_2$ | 1321 | 16.5 | 0.98 |
| M3 | 4933.25 | 148.1 | 14.8 | 0.37 | 0.004 | 0.0008 | 0.00008 | 0.00008 | 0.000038 | 0.000038 | 0.00012 | 0.002 | 0.00215 | 153 | $J_3$–$K_1$ | 4530 | 53.0 | 1.2 |
| M3 | 4933.25 | 128.3 | 11.7 | 0.32 | 0.007 | 0.0007 | 0.00006 | 0.00006 | 0.000033 | 0.000033 | 0.00010 | 0.002 | 0.00158 | 154 | $J_3$–$K_1$ | 4250 | 44.0 | 1.3 |

$C_1$: methane; $C_2$: ethane; $C_3$: propane; $iC_4$: isobutane; $nC_4$: n-butane; $iC_5$: isopentane; $nC_5$: n-pentane; $H_2$: hydrogen; $N_2$: nitrogen; $CO_2$: carbon dioxide. Th: homogenization temperature; $F_v$: gas-liquid ratio; Pt: Capture pressure; Pc: pressure coefficient.

### 4.7. Residual pressure differences between the source rock and reservoir during the critical natural gas charging periods

The residual pressure difference between the source rock of Xu-3 or Xu-5 member and the reservoir of Xu-4 member in the study area provided the driving force for natural gas charging. Table 3 and Fig. 10 shown the calculation results of residual pressure difference between the source rock of Xu-3 or Xu-5 member and the reservoir of Xu-4 member in the study area during the critical natural gas charging periods. On the whole, the residual pressure differences of Xu-3 member – Xu-4 member ranged from 0.1 to 21.4 MPa during the $J_2$, and from 17.5 to 33.2 MPa during the $J_3$ – the $K_1$. The residual pressure differences of Xu-5 member – Xu-4 member ranged from 0.2 to 9.9 MPa during the $J_2$, and from 14.5 to 28.4 MPa during the $J_3$ – the $K_1$.

On the plane, the residual pressure differences differed greatly in different regions and wells. During the $J_2$, the residual pressure differences of Xu-3 member – Xu-4 peaked near Wells YL171 and M101 (Fig. 10a), and that in the western region was higher than that in the eastern region. For the residual pressure differences of Xu-5 member – Xu-4 member, wells YB16 and YL171 were located at high values of residual pressure difference (Fig. 10b), and the difference of that between east and west was small. During the $J_3$ – the $K_1$, the residual pressure differences increased significantly, wells YL18, YB21, YB16 and YL28 were the highest value centers of residual pressure difference (Fig. 10c and d), and that of the western region was obviously higher than that of the eastern region.

## 5. Discussions

### 5.1. Formation and preservation of overpressure

#### 5.1.1. Distribution of overpressure of different causes

According to the analysis, the pressure distribution in Xujiahe Formation of the study area was characterized by large variation of overpressure interval and great difference in different wells (Figs. 3 and 5), exhibiting obvious heterogeneity, which were closely related to the generation and preservation of overpressure. By the logging identification of contributions of geological factors to overpressure and the relationship between formation pressure coefficient and total organic carbon (TOC) of source rocks with overpressure, it was believed that overpressure in the study area was mainly caused by tectonic compression and hydrocarbon generation. There are many overlapping distributions of logging data in the western and eastern regions in the study area in Fig. 5, reflecting both the hydrocarbon generation and the tectonic compression were the causes of overpressure. However, on the trend line of tectonic compression cause, the acoustic time difference in the eastern region becomes smaller and more obvious than that in the western region, indicating that there may be more tectonic compression cause in the eastern region.

We believe that this difference is the result of early overpressure formation and late overpressure release. The hydrocarbon generation in the western region is greater than that in the eastern region when the early overpressure formation, which makes the early overpressure unevenly distributed. The late tectonic compression resulted in the superposition of overpressure, but at the same time, faults were formed in the eastern region, and the early fluid expansion overpressure and late tectonic compression overpressure were released in a large scale, which made the strata of the eastern region mainly retain part of the late tectonic compression overpressure. The late tectonic compression overpressure in the western area were released when fractures were formed during next strong tectonic activities. Due to the

**Table 3**
Calculation results of different pressures of source rocks and reservoirs in northern Sichuan Basin.

| Region | Well | Residual pressure (MPa) | | Hydrocarbon generation pressure (MPa) | | | | Tectonic compression pressure (MPa) | | | | Residual pressure (MPa) | | | | Driving force for natural gas charging (MPa) | | | |
|---|---|---|---|---|---|---|---|---|---|---|---|---|---|---|---|---|---|---|---|
| | | Xu-4 member | | Xu-3 member | | Xu-5 member | | Xu-3 member | | Xu-5 member | | Xu-3 member | | Xu-5 member | | Xu-3 – Xu-4 | | Xu-5 – Xu-4 | |
| | | $J_2$ | $J_3$-$K_1$ | $J_2$ | $J_3$-$K_1$ | $J_2$ | $J_3$-$K_1$ | $J_2$ | $J_3$-$K_1$ | $J_2$ | $J_3$-$K_1$ | $J_2$ | $J_3$-$K_1$ | $J_2$ | $J_3$-$K_1$ | $J_2$ | $J_3$-$K_1$ | $J_2$ | $J_3$-$K_1$ |
| Western region | YB16 | 4.2 | 19.6 | 15 | 14.1 | 14.1 | 9.9 | 0 | 33.7 | 0 | 34.8 | 15 | 47.8 | 14.1 | 44.7 | 10.8 | 28.2 | 9.9 | 25.1 |
| | YL2 | 7.3 | 26.4 | 20.6 | 17.4 | 7.5 | 14.2 | 0 | 30.9 | 0 | 32 | 20.6 | 48.3 | 7.5 | 46.2 | 13.3 | 21.9 | 0.2 | 19.8 |
| | YL4 | 6.9 | 28 | 16.5 | 11.1 | 7.7 | 6.9 | 0 | 34.4 | 0 | 35.7 | 16.5 | 45.5 | 7.7 | 42.6 | 9.6 | 17.5 | 0.8 | 14.6 |
| | YL11 | 3 | 23.1 | 3.1 | 11.2 | 4.6 | 6.7 | 0 | 32.2 | 0 | 33.3 | 3.1 | 43.4 | 4.6 | 40 | 0.1 | 20.3 | 1.6 | 16.9 |
| | YL15 | 0.7 | 23.8 | 4.6 | 6.8 | 1.2 | 8.2 | 0 | 38.2 | 0 | 30.1 | 4.6 | 45 | 1.2 | 38.3 | 3.9 | 21.2 | 0.5 | 14.5 |
| | YL17 | 5.9 | 26.2 | 17.2 | 20 | 8.6 | 12.9 | 0 | 29 | 0 | 31.3 | 17.2 | 49 | 8.6 | 44.2 | 14 | 33.2 | 5.4 | 28.4 |
| | YL28 | 2.5 | 17.7 | 15.1 | 5.6 | 8.9 | 1.4 | 0 | 40.8 | 0 | 42.7 | 15.1 | 46.4 | 8.9 | 44.1 | 12.6 | 28.7 | 6.4 | 26.4 |
| | YL172 | 8.2 | 28.5 | 10.2 | 20.7 | 15.6 | 14.1 | 0 | 28.6 | 0 | 31.2 | 10.2 | 49.3 | 15.6 | 45.3 | 2 | 20.8 | 7.4 | 16.8 |
| | YL173 | 6.1 | 26.6 | 27.5 | 18 | 11.8 | 12.6 | 0 | 30.4 | 0 | 31.9 | 27.5 | 48.4 | 11.8 | 44.5 | 21.4 | 21.8 | 5.7 | 17.9 |
| Eastern region | M3 | 8.2 | 30 | 12.6 | 45.2 | 13.3 | 40.1 | 0 | 6.9 | 0 | 8.3 | 12.6 | 52.1 | 13.3 | 48.4 | 4.4 | 22.1 | 5.1 | 18.4 |
| | M201 | 7.5 | 21 | 19.1 | 6 | 8.3 | 1.7 | 0 | 30.9 | 0 | 33.2 | 19.1 | 36.9 | 8.3 | 34.9 | 17.1 | 22.2 | 6.3 | 20.2 |

$J_2$: Middle Jurassic; $J_3$-$K_1$: From Later Jurassic to Early Cretaceous.

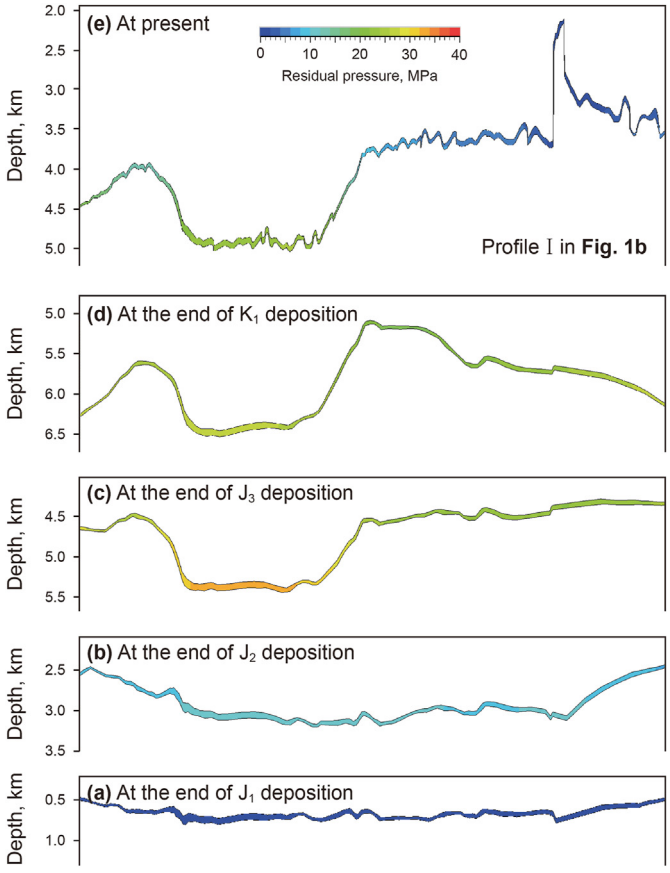


**Fig. 9.** Residual pressure evolution of the Xu-4 member reservoir in northern Sichuan Basin based on 2D simulation. The residual pressure exhibited an increasing trend from $J_2$ to $K_1$, during which there has the pressure decrease at the erosion period of $J_3$, and then decreasing from $K_2$ to present. The pressure in the eastern region decreased more rapidly rather than the western region from $K_2$ to present.

different distributions of faults and fractures, there are also changes in the causes of overpressure in a same area.

In addition to hydrocarbon generation and tectonic compression, the other geological factors such as disequilibrium compaction, chemical compaction and aquathermal effect may not be responsible for the formation of overpressure, and the reasons were analyzed below. In the previous researches, it is believed that disequilibrium compaction overpressure occurs when the formation sedimentation rate is over 200 m/Ma (Wang et al., 2021). However, in the western and eastern areas of the study area, the average formation sedimentation rate in the Mesozoic was 66 m/Ma and 87 m/Ma, respectively, so disequilibrium compaction was difficult to occur. And the variation of logging parameters of overpressured formation is not consistent with the logging response of disequilibrium compaction formation. Chemical compaction including clay mineral transformation is affected by time, temperature, mineral composition and other factors, and the logging response shows a trend of decreasing acoustic travel time and increasing density (Li and Luo, 2017). However, the logging response of overpressured formation in the study area shows no obvious trend of increasing density. Therefore, chemical compaction is not the main cause of overpressure in the study area.

In addition, aquathermal effect caused by temperature increase mainly occurs in the early tectonic subsidence stage. Under the action of fluid pressure difference, water can migrate through reservoir with small pore throats and lead to pressure leakage, so the effect of aquathermal pressurization is relatively limited, while the positive correlation between overpressure and TOC also shows that hydrocarbon generation rather than aquathermal effect is the main reason for overpressure of fluid expansion. According to the 2D simulation of residual pressure evolution history, the lateral pressures at different periods present a gradual change, reflecting the existence of overpressure transfer in the lateral direction. However, in the identification chart of overpressure causes (Fig. 5), it is difficult to identify the existence of overpressure transfer directly because the logging responses of overpressure transfer are similar to that of fluid expansion overpressure.

### 5.1.2. Geological factors affecting the formation of overpressure in key periods

Source rocks of Xu-3 member and Xu-5 member in the study area were characterized by large-scale distribution and large thickness (Zou et al., 2009; Zhao et al., 2011), providing conditions for large-scale hydrocarbon generation, and large-scale overpressure can be produced in closed systems (Spencer, 1987; Hao et al., 2007; Feyzullayev and Lerche, 2009). By comparison, the degree of thermal evolution of the source rocks of the Xujiahe Formation in the western and eastern regions of the study area during the $J_2$ was low, and there was only a small-scale overpressure generated. During the $J_3$ – $K_1$, although the degree of

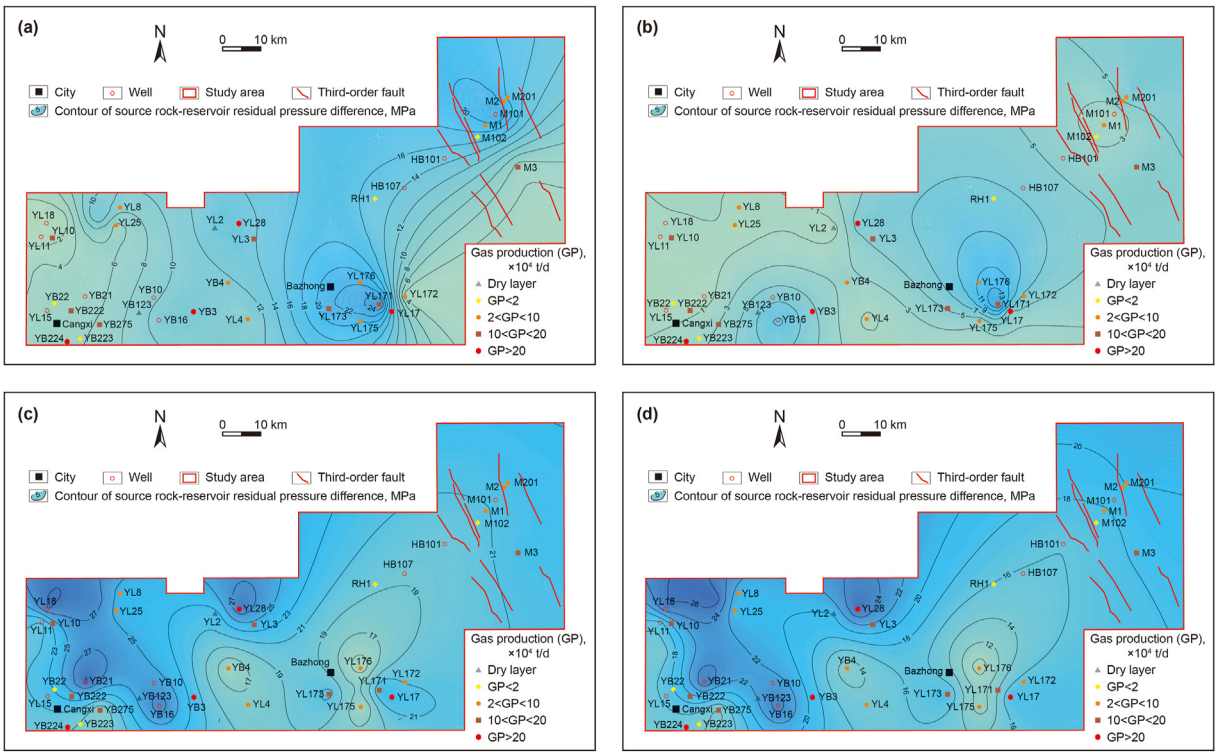


**Fig. 10.** Distributions of source rock-reservoir residual pressure differences during the critical natural gas charging periods and their relationship with gas production of reservoir in northern Sichuan Basin. (a), (c) Represent the residual pressure difference between Xu-3 member source rock and Xu-4 member reservoir during $J_2$, $J_3 - K_1$, respectively. (b), (d) Represent the residual pressure difference between Xu-5 member source rock and Xu-4 member reservoir during $J_2$, $J_3 - K_1$, respectively. By comparison, the wells with large daily gas production were mainly located in the area with large residual pressure differences in the western region, while the daily gas production was not only controlled by residual pressure difference, but also controlled by the third-order fault in the eastern region.

thermal evolution of the source rocks in the eastern region was higher than that in the western region, the development of the source rocks in the western region was higher than that in the eastern region, for example, the total thickness of the dark mudstone source rocks of Xu-3 and Xu-5 member in the western region of the study area was more than 100 m, while only the eastern edge of the source rocks in the eastern region was more than 100 m. As a result, the degree of pressure increase of source rocks of Xujiahe Formation in the western region was still higher than that in the eastern region.

In addition to the hydrocarbon generation pressure, the Middle Yanshan movement in the $J_3 - K_1$ had a strong compressive effect on the study area, forming a relatively large amount of tectonic compression pressure (Zeng et al., 2010), and there were some differences in the amounts of tectonic compression pressure for different tectonic parts. Therefore, the difference between the hydrocarbon generation pressure and tectonic compression pressure at different regions in the study area was an important reason for the difference in overpressure development during the critical periods of natural gas charging. However, the tectonic movement since the $K_2$ had resulted in a significantly stronger tectonic deformation in the east than in the west, resulting that only small-scale fourth-order faults were developed in the western region, while a large number of third-order and fourth-order faults were developed in the eastern region. Therefore, the overpressure preservation condition in the eastern region was worse than that in the western region, leading to more overpressure leakage in the eastern region. Consequently, the current overpressure distribution in the west was larger than that in the east.

### 5.1.3. Preservation conditions of overpressure

After the overpressure was formed, if the preservation conditions were not ideal, it would disappear in a short time (Muggeridge et al., 2005). Comparative analysis shows that both third-order and fourth-order faults were developed in the eastern region of the study area, while only fourth-order faults were developed in the western region.

As shown in Fig. 1c, the third-order faults are large in size, cut through multiple horizons and end up in the Upper Jurassic, while the fourth-order faults are small in size, have few cutting horizons and most of them develop in the Xujiahe Formation or end up in the Ziliujing Formation of Lower Jurassic (Fig. 1c). In the area with strong compression, the third-order faults or fourth-order faults tend to have two opposite tendencies and combine with the strata to form thrusting structures. In the areas with relatively weak compressive strength, fault spreading folds composed of fourth-order faults are often developed. The dip angles of third-order faults and fourth-order faults in the western and eastern regions of the study area are large, with most of them over 60°. However, most third-order faults have a fault displacement of more than 100 m, with an average fault displacement of about 353 m, while the fourth-order faults have a fault displacement range of 17–204 m, with an average fault displacement of about 48 m (Jiang et al., 2020), so the third-order faults were significantly more active than the fourth-order faults. It was believed that the faults in the study area were mainly formed in the Late Cretaceous (100 – 70 Ma) and Eocene-Oligocene (40 – 25 Ma), and were the result of strong compressive tectonic movement (Chen et al., 2017; Liu et al., 2019; Wen and Li, 2020). Because the overpressure of hydrocarbon generation had been formed in the source rocks during these two periods, the process of overpressure release should have been

occurred under the condition of faults development. Meanwhile, the tectonic compression overpressure was also formed by the strong compression movement, and this kind of overpressure may also be leaked along these faults.

Although there were strong tectonic movements in the study area and the overpressure had been released to an extent, there had still an overpressure with a pressure coefficient of 2.16 locally, the reason was closely related to the densification of Xu-4 member reservoir. The reservoir of Xu-4 member in the Xujiahe Formation in the study area was abnormally tight, with porosities of 1%–4% and permeability of 0.001–0.1 mD. For the Xu-4 member reservoir, it was observed that it had experienced compaction diagenesis during the $J_2$, reducing the porosity to 15% at the end of $J_2$, and strong cementation from $J_3$ to $K_1$ further densified the reservoir, reducing the porosity to below 10% at the end of $J_3$, and below 5% at the end of $K_1$ (Fig. 11). Therefore, during the main natural gas generating and charging period ($J_3$-$K_1$), most of the reservoir was already densified (Fig. 11), making it was conducive to the preservation of overpressure. In addition, the reservoir of Xu-4 member was located between Xu-3 and Xu-5 members source rocks, and had the conditions of upper and lower sealing layers, which was also one of the reasons why overpressure can be partly preserved.

### 5.2. Relationship of overpressure evolution between source rocks and reservoir, and its control on natural gas distribution

Tight sandstone reservoirs generally distributed close to source rocks (Tong et al., 2012), and the residual pressure difference between source rock and reservoir was the driving force for tight sandstone gas charging (Zhang et al., 2012; Li and Li, 2010). The evolution of residual pressure difference was controlled by the overpressure evolution of source rock and reservoir (Fig. 12). By comparison, the reservoir pressure at different geological times was lower than that of the source rock, but the reservoir exhibited a similar pressure evolution trend to the source rock, reflecting that the reservoir pressure evolution was controlled by the source rock pressure evolution to some extent. The overpressure differences of Xu-3 member source rock – Xu-4 member reservoir and Xu-5 member source rock – Xu-4 member reservoir were the driving force for tight sandstone gas charging, it also shown a trend of increasing first and then decreasing, which was consistent with the pressure evolution of source rock and reservoir. During the critical periods of natural gas charging ($J_2$ and $J_3 - K_1$), the driving force was relatively large, serving as an ideal condition for natural gas migration from the source rocks of Xu-3 member and Xu-5 member to the reservoir of Xu-4 member.

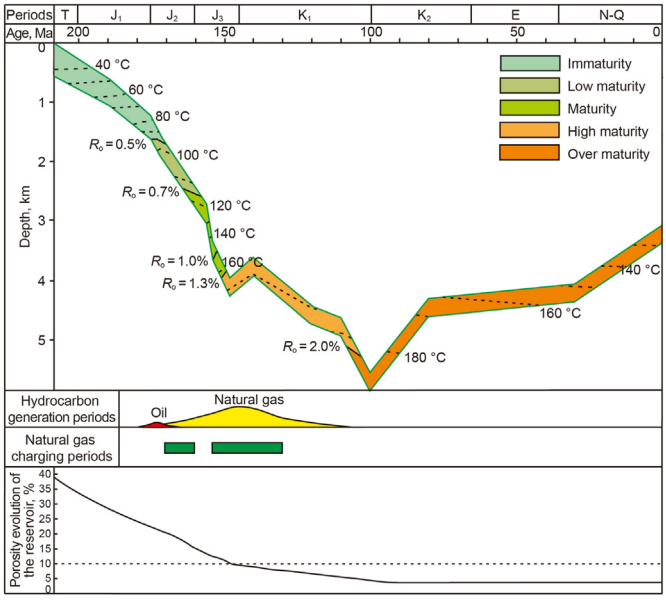


**Fig. 11.** Pore evolution history of the Xu-4 member reservoir and its relationship with natural gas generating and charging periods in northern Sichuan Basin.

According to the analysis of the causes of overpressure in Section 5.1, the hydrocarbon generation pressure and tectonic compression pressure of Xu-3 and of Xu-5 members were considered to be the main causes of overpressure, which were therefore the main reasons for the formation of the driving force for natural gas charging. By the comparison of the differences in the horizontal distribution of driving force during the key charging periods, it was believed that the largest centers of driving force were in the proximity of Wells YL18-YB21-YB16, YL28, YL17-YL171 and M101, which were largely consistent with the distribution of source rocks. Controlled by the distribution of source rocks and driving force differences, the distribution of natural gas in the study area shown obvious differences in its enrichment and distribution. Wells with a daily gas production (GP) of $(2–10) \times 10^4$ t/d, $(10–20) \times 10^4$ t/d or $>20 \times 10^4$ t/d in the western region of the study area were mainly located in wells YL18-YB21-YB16, YL28 and YL17-YL171, which was mainly because that these areas have a larger scale of natural gas generation during the critical periods, forming a great driving force, then controlling the charging and enrichment of natural gas. However, there was no obvious positive correlation between the driving force and wells in the eastern region with a daily gas production (GP) of $(2–10) \times 10^4$ t/d or $(10–20) \times 10^4$ t/d, which was mainly due to the existence of large-scale third-order faults (Fig. 10) in this region, The faults extended downwards to the Permian marine source rocks (Cao et al., 2018), which was conducive to the upward migration of underlying natural gas into the Xu-4 member reservoir of Xujiahe Formation. Although the third-order fault was conducive to the charging of natural gas from Permian marine source rocks, the faults had an adverse effect on the natural gas preservation, resulting the pressure in the eastern region dissipated to a greater extent. Therefore, the most favorable area for natural gas charging was the western region of the study area, where the source rocks were developed and the natural gas driving force was sufficient.

### 5.3. Control of driving force on effective pore throat of natural gas charging

The driving force during natural gas charging periods played an important role in controlling the efficiency of natural gas migration and accumulation (Anissimov, 2001; Zhang et al., 2009; Sun et al., 2008), and the amount of the driving force often determined the pore throat radius of natural gas charging. The statistical results shown that the Xu-4 member of Xujiahe Formation in the western region of the study area had driving forces ranged from 0.1 to 21.4 MPa in the $J_2$ and from 14.5 to 33.2 MPa in the $J_3 - K_1$. By calculation of the relationship between the driving force and the capillary resistance ($r = 2\sigma\cos(\theta)/P$, where $r$ is the pore throat radius, μm; $\sigma$ is the gas-water interfacial tension, 25 mN/m at 140 °C (Bao, 1988); $\theta$ is contact angle, 140°; $P$ is the driving force, MPa), the minimum pore throat radius of natural gas charging were 1.8–383 nm in the $J_2$ and 1.2–2.6 nm in the $J_3 - K_1$. In the eastern region, however, the driving forces of Xu-4 member of Xujiahe Formation ranged from 4.4 to 17.1 MPa in the $J_2$ and from 18.4 to 22.2 MPa in the $J_3 - K_1$. The minimum pore throat radius of natural gas charging were 2.8–8.7 nm in the $J_2$ and 1.7–2.2 nm in the $J_3 - K_1$ (Fig. 13). By comparing the above results, it could be seen that under the control of the driving force, the lower limit of natural gas

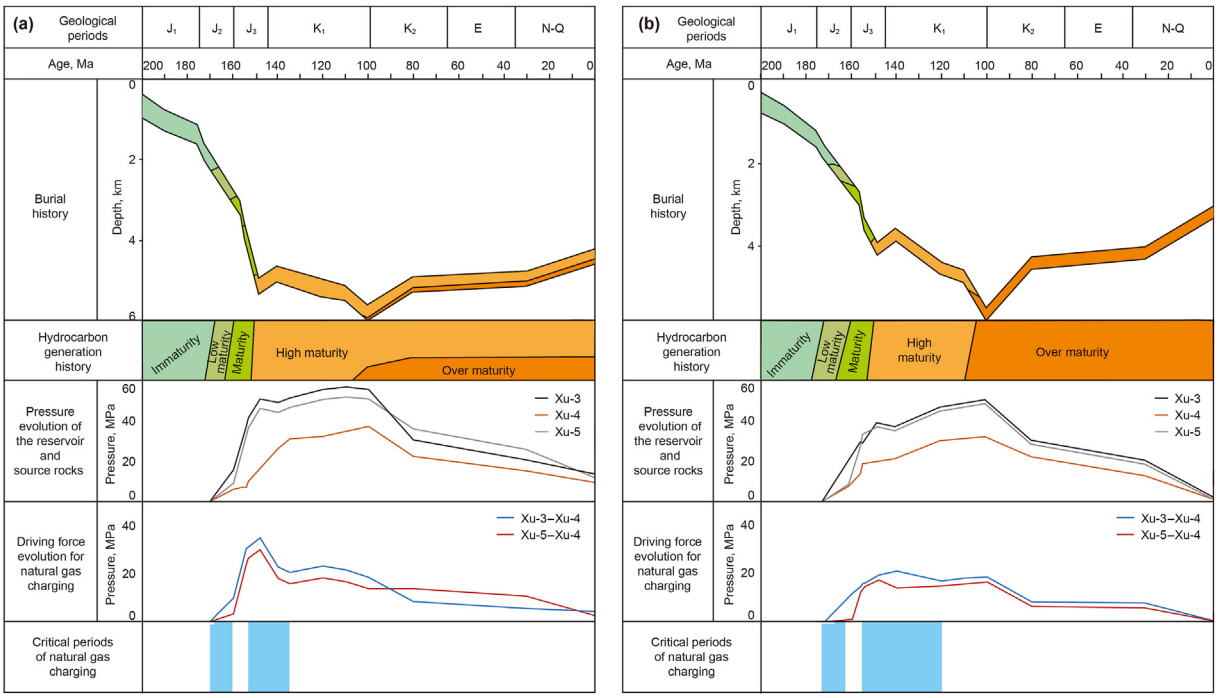


**Fig. 12.** Comprehensive analytical diagrams of driving force for natural gas charging of the Xu-4 member in northern Sichuan Basin. (a), (b) Represent the western region; (c), (d) represent the eastern region. The evolutions of pressure of Xu-4 member and driving force for natural gas charging were controlled by pressure evolution of source rocks. During the second critical period of natural gas charging ($J_3 - K_1$), the driving force was enough to drive large natural gas migration from the Xu-3 and Xu-5 members to Xu-4 member.

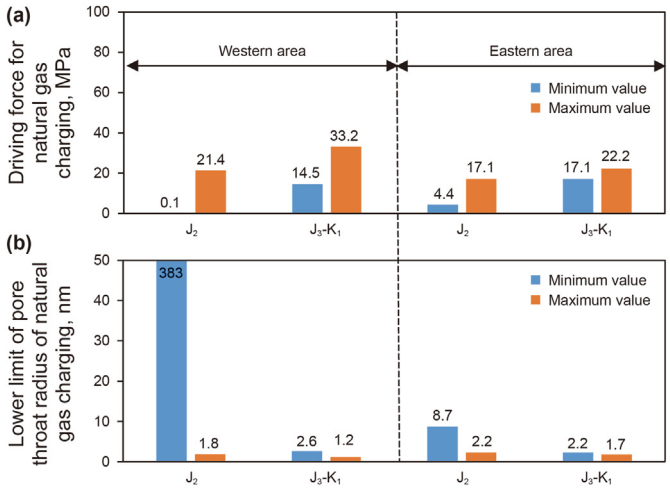


**Fig. 13.** Comparisons of driving force for natural gas charging (a) and lower limit of charging pore throat radius (b) in the critical charging periods. The amount of the driving force determined the pore throat radius of natural gas charging. The lower limit of natural gas charging pore throat radius during the $J_3 - K_1$ was significantly lower than that during the $J_2$.

charging pore throat in the $J_3 - K_1$ was significantly lower than that in the $J_2$, but the Xu-4 member reservoir had a large effective charging space both during $J_2$ and $J_3 - K_1$.

According to the above data of driving force and the lower limit of pore throat of natural gas charging, the relation diagram (Fig. 14) between them was made. As the driving force increases, lower limit of pore throat decreases. According to the driving force distribution of Xu-4 reservoir in $J_2$ and $J_3$–$K_1$ periods, only local area occurred gas charging in $J_2$ period, while gas was widely charged in $J_3$–$K_1$ period. However, the lower limit of pore throat of natural gas charging was also large in areas with large driving force.

The Xu-4 member reservoir of the Xujiahe Formation in the study area was tight lithic sandstone and feldspar lithic sandstones, and the pore throat radiuses of the reservoir were distributed from 0.005 to 10 μm, whose main distribution range was 0.01–0.5 μm. When the driving force is greater than 4 MPa, natural gas can be charged into all reservoir spaces with pore throat radius greater than 10 nm. So the difference of natural gas charging by the driving force was also an important factor resulted in the difference of natural gas enrichment.

## 6. Conclusions

Through statistics and comparison of Xu-4 member of Xujiahe Formation in northeastern Sichuan Basin, the pressures ranged from 37.0 to 93.6 MPa, the pressure coefficients ranged from 1.04 to 2.22, and the overpressure in the western region was larger than that in the eastern region on the whole. Hydrocarbon generation and tectonic compression were the main causes for overpressure in the study area, but the contributions of the two causes to overpressure were different in different periods and areas. Hydrocarbon generation is the most important one in the $J_2$, while both hydrocarbon generation and tectonic compression were important in the $J_3 - K_1$. For the developmental differences between the two causes in different formations, the overpressure amount of Xu-3 member was higher than that of Xu-5 member. Affected by the tectonic movement since the $K_2$, the tectonic deformation in the eastern region was significantly stronger than that in the western region, resulting in a rapid pressure decrease in the eastern region.

According to the research of overpressure evolution, it was believed that the pressure evolution trend of the reservoir of Xu-4 member was consistent with that of the source rock of Xu-3 and Xu-5 members in study area, but the amount of overpressure of the reservoir was lower than that of the source rocks. Therefore, the source-reservoir residual pressure difference during the critical

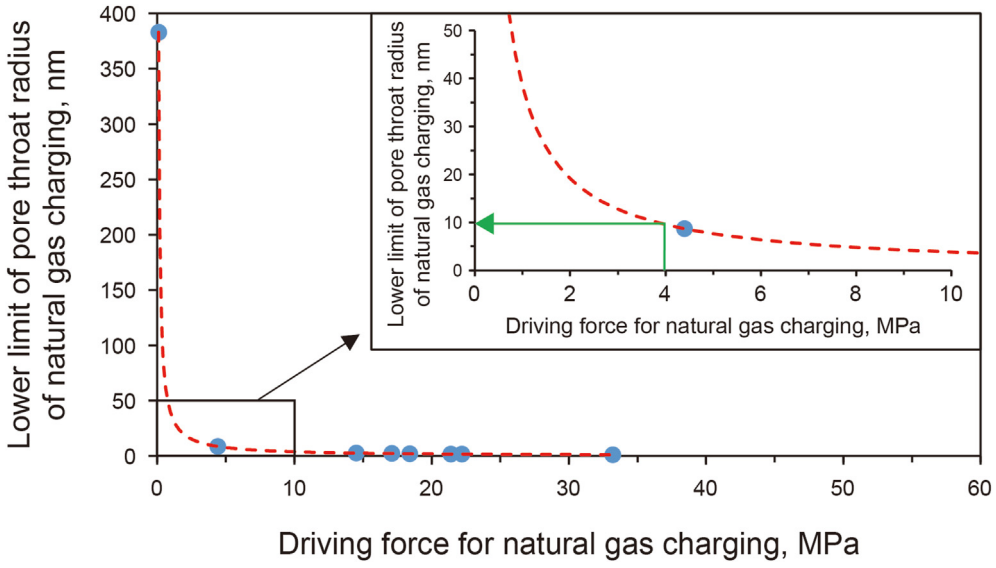


**Fig. 14.** Relationship of driving force for natural gas charging and lower limit of charging pore throat radius in the critical charging periods in the study area.

charging periods was the main driving force for natural gas charging, and its evolution trend was consistent with that of the source rocks and reservoir. For the study area, the natural gas driving force was large and was favorable for the natural gas charging from the source rocks to the reservoir during the $J_2$ and the $J_3 - K_1$. Controlled by the difference of the driving force in different areas, the areas with high hydrocarbon generation of source rocks and low tectonic activity were entirely rich in natural gas. Meanwhile, the driving force determined the effective pore throat space of natural gas charging.

## Acknowledgements

This study was financially supported by the Development Fund of Shandong Provincial Key Laboratory of Deep Oil and Gas, the Fundamental Research Funds for the Central Universities (20CX02110A), and the National Natural Science Foundation of China (41702142).

## References

Amyx, J.W., Bass, D.M., Whiting, R.L., 1960. Petroleum Reservoir Engineering: Physical Properties. McGraw-Hill, New York.
Anissimov, L., 2001. Overpressure phenomena in the precaspian basin. Petrol. Geosci. 7 (4), 389–394. https://doi.org/10.1144/petgeo.7.4.389.
Aplin, A.C., Macleod, G., Larter, S.R., Pedersen, K.S., Sorensen, H., Booth, T., 1999. Combined use of Confocal Laser Scanning Microscopy and PVT simulation for estimating the composition and physical properties of petroleum in fluid inclusions. Mar. Petrol. Geol. 16 (2), 97–110. https://doi.org/10.1016/S0264-8172(98)00079-8.
Bao, C., 1988. Geology of Natural Gas. Science Press, Beijing (in Chinese).
Bera, A., Shah, S., 2021. A review on modern imaging techniques for characterization of nanoporous unconventional reservoirs: challenges and prospects. Mar. Petrol. Geol. 133, 105287. https://doi.org/10.1016/j.marpetgeo.2021.105287.
Bourdet, J., Pironon, J., Levresse, G., Tritlla, J., 2010. Petroleum accumulation and leakage in a deeply buried carbonate reservoir, Níspero field (Mexico). Mar. Petrol. Geol. 27 (1), 126–142. https://doi.org/10.1016/j.marpetgeo.2009.07.003.
Bowers, G.L., 2002. Detecting high overpressure. Lead. Edge 21 (2), 174–177. https://doi.org/10.1190/1.1452608.
Cao, H.Y., Wang, W., Liu, M., 2018. Characteristics of fractures in Xujiahe formation of Tongnanba structural belt, northeastern Sichuan Basin. Xinjing Pet. Geol. 39 (4), 424–429. https://doi.org/10.7657/XJPG20180407 (in Chinese).
Cao, L., 2010. Gas Accumulation Dynamics of Tight Sandstone Reservoir-Example from the Upper Xujiahe Formation in Western Sichuan Depression. Chengdu University of Technology, Chengdu (in Chinese).
Chen, L.B., He, D.F., Wang, B., Li, Y.Q., Mei, Q.H., Wen, Z., 2017. Dating the tectonic deformation since the middle Triassic for the Tongnanba anticline in the northeastern Sichuan Basin and its geological implications. Geotect. Metallogenia 41 (3), 433–445. https://doi.org/10.16539/j.ddgzyckx.2017.03.001.
Dai, J.X., Ni, Y.Y., Wu, X.Q., 2012. Tight gas in China and its significance in exploration and exploitation. Petrol. Explor. Dev. 39 (3), 277–284. https://doi.org/10.1016/S1876-3804(12)60043-3.
Dai, J.X., Ni, Y.Y., Zou, C.N., Tao, S.Z., Hu, G.Y., Hu, A.P., Yang, C., Tao, X.W., 2009. Stable carbon isotopes of alkane gases from the Xujiahe coal measures and implication for gas-source correlation in the Sichuan Basin, SW China. Org. Geochem. 40 (5), 638–646. https://doi.org/10.1016/j.orggeochem.2009.01.012.
Dong, D.Z., Gao, S.K., Huang, J.L., Guan, Q.Z., Wang, S.F., Wang, Y.M., 2014. A discussion on the shale gas exploration and development prospect in the Sichuan Basin. Nat. Gas. Ind. 31 (12), 1–15. https://doi.org/10.1016/j.ngib.2015.02.002 (in Chinese).
Dubow, J., 1984. Temperature effects. In: Chong, K.P., Smith, J.W. (Eds.), Mechanics of Oil Shale. Elsevier Applied Science Publishers, London, pp. 523–577.
Eaton, B.A., 1975. The Equation for Geopressure Prediction from Well Logs. 50th Annual Fall Meeting of the Society of Petroleum Engineers of AIME, Texas.
Feyzullayev, A.A., Lerche, I., 2009. Occurrence and nature of overpressure in the sedimentary section of the south Caspian Basin. Azerbaijan Energy Explor. Explvoitation. 27 (5), 345–366. https://doi.org/10.1260/0144-5987.27.5.345.
Guo, X.W., Liu, K.Y., He, S., Yang, Z., Dong, T.T., 2016. Quantitative estimation of overpressure caused by gas generation and application to the baiyun depression in the pearl river mouth basin, south China sea. Geofluids 16 (1), 129–148. https://doi.org/10.1111/gf1.12140.
Guo, Y.C., Song, Y., Pang, X.Q., Wang, Y.W., Yang, K.M., Li, B.Y., 2015. Hydrocarbon generation and expulsion of the Upper Triassic $T_3x^5$ source rocks in the western Sichuan Depression: assessment for unconventional natural gas. Acta Geol. Sin. 89 (1), 175–186. https://doi.org/10.1111/1755-6724.12403 (in Chinese).
Hao, F., 2005. Kinetic of Hydrocarbon Generation and Mechanisms of Petroleum Accumulation in Overpressured Basin. Science Press, Beijing (in Chinese).
Hao, F., Li, S.T., Dong, W.L., Hu, Z.L., Huang, B.J., 2007. Abnormal organic-matter maturation in the Yinggehai Basin, South China Sea: implications for hydrocarbon expulsion and fluid migration from overpressured systems. J. Petrol. Geol. 21 (4), 427–444. https://doi.org/10.1111/j.1747-5457.1998.tb00794.x.
Jia, C.Z., Zheng, M., Zhang, Y.F., 2012. Unconventional hydrocarbon resources in China and the prospect of exploration and development. Petrol. Explor. Dev. 39 (2), 139–146. https://doi.org/10.1016/S1876-3804(12)60026-3.
Jiang, Y.L., Li, M.Y., Wang, L.J., Zeng, T., Liu, J.D., Li, J., 2020. Controlling effect of faults on tight sandstone natural gas accumulation and enrichment in Tongnanba Area, Northeast Sichuan. J. Univ. Pet., China (Ed. Nat. Sci.) 44 (5), 19–31. https://doi.org/10.3969/j.issn.1673-5005.2020.05.003 (in Chinese).
Jin, W.Z., Tan, L.J., Yan, K.M., Wan, G.M., Lv, Z.Z., Yu, Y.X., 2009. Tectonic evolution of the middle frontal area of the longmen mountain thrust belt, western Sichuan Basin, China. Acta Geol. Sin. 83 (1), 92–102. https://doi.org/10.1111/j.1755-6724.2009.00011.x (in Chinese).
Karlsen, D., Nedkvitne, T., Larter, S.R., Bjorlykke, K., 1993. Hydrocarbon composition of authigenic inclusions: applications to elucidation of petroleum reservoir filling history. Geochem. Cosmochim. Acta 57 (15), 3641–3659. https://doi.org/10.1016/0016-7037(93)90146-n.
Krakowska, P., Puskarczyk, E., Jędrychowski, M., Habrat, M., Madejski, P., Dohnalik, M., 2018. Innovative characterization of tight sandstones from Paleozoic basins in Poland using X-ray computed tomography supported by nuclear magnetic resonance and mercury porosimetry. J. Petrol. Sci. Eng. 166, 389–405. https://doi.org/10.1016/j.petrol.2018.03.052.

Kuhn, P.P., Primio, R.D., Hill, R., Lawrence, J.R., Horsfield, B., 2012. Three-dimensional modeling study of the low-permeability petroleum system of the Bakken Formation. AAPG (Am. Assoc. Pet. Geol.) Bull. 96 (10), 1867–1897. https://doi.org/10.1306/03261211063.

Law, B.E., Curtis, J.B., 2002. Introduction to unconventional petroleum systems. AAPG (Am. Assoc. Pet. Geol.) Bull. 86 (11), 1851–1852. https://doi.org/10.1306/61EEDDA0-173E-11D7-8645000102C1865D.

Li, C., Luo, X.R., 2017. Review on mudstone chemical compaction. J. Earth Sci. Environ. 39 (6), 761–772 (in Chinese).

Li, J., Zou, H.Y., Zhang, G.C., Li, P.P., Feng, C., Zhang, Y.Z., Chen, J.S., 2012. Origins of overpressure tight gas reservoirs in the Xujiahe Formation, northeastern Sichuan Basin. J. Jilin Univ. (Earth Sci. Ed.) 42 (3), 624–633. https://doi.org/10.13278/j.cnki.jjuese.2012.03.003 (in Chinese).

Li, M.C., Li, J., 2010. "Dynamic trap": a main action of hydrocarbon charging to form accumulations in low permeability-tight reservoir. Acta Pet. Sin. 31 (5), 718–722. https://doi.org/10.7623/syxb201005003 (in Chinese).

Liu, J.D., Li, L., Zhang, C.J., Jiang, Y.L., Swennen, R., Zhao, C.J., Hou, S., 2022a. Identification and quantitative evaluation of pores and throats of a tight sandstone reservoir (Upper Triassic Xujiahe Formation, Sichuan Basin, China). Mar. Petrol. Geol. 140, 105663. https://doi.org/10.1016/j.marpetgeo.2022.105663.

Liu, J.D., Liu, T., Liu, H., He, L.L., Zheng, L.J., 2021. Overpressure caused by hydrocarbon generation in the organic-rich shales of the Ordos Basin. Mar. Petrol. Geol. 134, 105349. https://doi.org/10.1016/j.marpetgeo.2021.105349.

Liu, J.D., Zhang, C.J., Jiang, Y.L., Hou, S., 2022b. Investigation on pore structure characteristics of ultra-tight sandstone reservoirs in the upper Triassic Xujiahe Formation of the northern Sichuan Basin, China. Mar. Petrol. Geol. 138, 105552. https://doi.org/10.1016/j.marpetgeo.2022.105552.

Liu, Q.Y., Jin, Z.J., Meng, Q.Q., Wu, X.Q., Jia, H.C., 2015. Genetic types of natural gas and filling patterns in Daniudi gas field, Ordos Basin, China. J. Asian Earth Sci. 107, 1–11. https://doi.org/10.1016/j.jseaes.2015.04.001.

Liu, T., Liu, J.D., 2018. Quantitative evaluation on overpressure generated from undercompaction and fluid expansion. Acta Pet. Sin. 39 (9), 971–979. https://doi.org/10.7623/syxb201809002 (in Chinese).

Liu, Z.Q., Luo, K.P., Tang, Y., Yang, F., Mei, L.F., Shen, C.B., 2019. Critical tectonic periods and the response of gas accumulation in Non-Marine tight sandstone reservoir in Yuanba-Tongnanba area, Sichuan Basin. Earth Sci. 44 (3), 756–772. https://doi.org/10.3799/dqkx.2019.032 (in Chinese).

Luo, X.R., Wang, Z.M., Zhang, L.Q., Yang, W., Liu, L.J., 2007. Overpressure generation and evolution in a compressional tectonic setting, the southern margin of Junggar Basin, northwestern China. AAPG (Am. Assoc. Pet. Geol.) Bull. 91 (8), 1123–1139. https://doi.org/10.1306/02260706035.

Ma, X.H., Jia, A.L., Tan, J., He, D.B., 2012. Tight sand gas development technology and practices in China. Petrol. Explor. Dev. 39 (5), 611–618. https://doi.org/10.1016/S1876-3804(12)60083-4.

Ma, Y.S., Guo, X.S., Guo, T.L., Huang, R., Cai, X.Y., Li, G.X., 2007. The Puguang gas field: new giant discovery in the mature Sichuan Basin, Southwest China. AAPG (Am. Assoc. Pet. Geol.) Bull. 91 (5), 627–643. https://doi.org/10.1306/11030606062.

McCain, W.D., 1990. The Properties of Petroleum Fluids. PennWell, Oklahoma.

Meckel, L.D., Thomasson, M.R., 2005. Pervasive tight-gas sandstone reservoirs; an overview. AAPG Hedberg Series 3, 13–27. https://doi.org/10.1306/13131047h33321.

Muggeridge, A., Abacioglu, Y., England, W., Smalley, C., 2005. The rate of pressure dissipation from abnormally pressured compartments. AAPG (Am. Assoc. Pet. Geol.) Bull. 89 (1), 61–80. https://doi.org/10.1306/07300403002.

Osborne, M.J., Swarbrick, R.E., 1997. Mechanisms for generating overpressure in sedimentary basins: a reevaluation. AAPG (Am. Assoc. Pet. Geol.) Bull. 81 (6), 1023–1041. https://doi.org/10.1306/522B49C9-1727-11D7-8645000102C1865D.

Qin, S.F., Li, F., Li, W., Zhou, Z., Zhou, G.X., 2018. Formation mechanism of tight coal-derived-gas reservoirs with medium-low abundance in Xujiahe Formation, central Sichuan Basin, China. Mar. Petrol. Geol. 89, 144–154. https://doi.org/10.1016/j.marpetgeo.2017.06.032.

Rezaee, R., Saeedi, A., Clennell, B., 2012. Tight gas sands permeability estimation from mercury injection capillary pressure and nuclear magnetic resonance data. J. Petrol. Sci. Eng. 88–89, 92–99. https://doi.org/10.1016/j.petrol.2011.12.014.

Rogner, H.H., 1997. An assessment of world hydrocarbon resources. Annu. Rev. Energy Environ. 22 (1), 369–382. https://doi.org/10.1146/annurev.energy.22.1.217.

Shanley, K.W., Cluff, R.M., 2015. The evolution of pore-scale fluid-saturation in low permeability sandstone reservoirs. AAPG (Am. Assoc. Pet. Geol.) Bull. 99, 1957–1990. https://doi.org/10.1306/03041411168.

Shen, C.B., Mei, L.F., Xu, S.H., 2009. Fission track dating of Mesozoic sandstones and its tectonic significance in the eastern Sichuan Basin, China. Radiat. Meas. 44 (9–10), 945–949. https://doi.org/10.1016/j.radmeas.2009.10.001.

Shi, M.X., Liu, Z.D., Yang, X.F., Yang, J.R., Chen, X.J., Liu, H.Z., Cao, J.L., 2020. Review and prospect prediction technology for formation pore pressure by geophysical well logging. Prog. Geophys. 35 (5), 1845–1853, 10. 6038/pg2020DD0435 (in Chinese).

So, B.D., Yuen, D.A., 2015. Generation of tectonic over-pressure inside subducting oceanic lithosphere involving phase-loop of olivine-wadsleyite transition. Earth Planet Sci. Lett. 413, 59–69. https://doi.org/10.1016/j.epsl.2014.12.048.

Spencer, C.W., 1987. Hydrocarbon generation as a mechanism for overpressuring in Rocky Mountain region. AAPG (Am. Assoc. Pet. Geol.) Bull. 71 (4), 368–388. https://doi.org/10.1306/94886EB6-1704-11D7-8645000102C1865D.

Sun, M.L., Liu, G.D., Li, J., 2008. Relationship between excess-pressure gradient and gas accumulation in overpressured basin. J. Univ. Pet., China (Ed. Nat. Sci.) 32 (3), 19–22. https://doi.org/10.3321/j.issn:1673-5005.2008.03.004.

Tao, S.Z., Gao, X.H., Li, C.W., Zeng, J.H., Zhang, X.X., Yang, C., Zhang, J.Y., Gong, Y.J., 2016. The experiment simulation study on gas percolation mechanisms of tight sandstone core in coal measure strata: a case study on coal-measure tight sandstone gas in the Upper Triassic Xujiahe Formation Sichuan Basin, China. Nat. Gas Geosci. 27 (7), 1143–1152. https://doi.org/10.11764/j.issn.1672-1926.2016.07.1143 (in Chinese).

Tingay, M.R.P., Hillis, R.R., Swarbrick, R.E., Morley, C.K., Damit, A.R., 2009. Origin of overpressure and pore-pressure prediction in the Baram province, Brunei. AAPG (Am. Assoc. Pet. Geol.) Bull. 93 (1), 51–74. https://doi.org/10.1306/08080808016.

Tong, X.G., Guo, B.C., Li, J.Z., Huang, X.F., 2012. Comparison study on accumulation and distribution of tight sandstone gas between China and the United States and its significance. Eng. Sci. 14 (6), 9–15. https://doi.org/10.3969/j.issn.1009-1742.2012.06.002.

Wang, Q.C., Chen, D.X., Gao, X.Z., Wang, F.W., Li, S., Tian, Z.Y., Lei, W.Z., Chang, S.Y., Zou, Y., 2021. Evolution of abnormal pressure in the Paleogene Es3 Formation of the huimin depression, bohai bay basin, China. J. Petrol. Sci. Eng. 203, 108601. https://doi.org/10.1016/j.petrol.2021.108601.

Wang, Y., Qiu, N., Borjigin, T., Shen, B., Xie, X., Ma, Z., Lu, C., Yang, Y., Yang, L., Cheng, L., Fang, G., Cui, Y., 2018. Integrated assessment of thermal maturity of the upper ordovician-lower silurian wufeng-longmaxi shale in Sichuan Basin, China. Mar. Petrol. Geol. 100, 447–465. https://doi.org/10.1016/j.marpetgeo.2018.10.025.

Wang, Z.C., Jiang, H., Wang, T.S., Lu, W.H., Gu, Z.D., Xu, A.N., Yang, Y., Xu, Z.H., 2014. Paleo-geomorphology formed during Tongwan tectonization in Sichuan Basin and its significance for hydrocarbon accumulation. Petrol. Explor. Dev. 41 (3), 338–345. https://doi.org/10.1016/S1876-3804(14)60038-0.

Wang, Z.L., Zhang, L.K., Shi, L.Z., Sun, M.L., 2005. Genesis analysis and quantitative evaluation on abnormal high fluid pressure in the kela-2 gas field, kuqa depression, tarim basin. Geol. Rev. 51 (1), 55–63. https://doi.org/10.3321/j.issn:0371-5736.2005.01.008.

Wei, X.S., Hu, A.P., Zhao, H.T., Kang, R., Shi, X.Y., Liu, X.P., 2017. New geological understanding of tight sandstone gas. Lithologic Reservoirs 29 (1), 11–20. https://doi.org/10.3969/j.issn.1673-8926.2017.01.002 (in Chinese).

Wen, K., Li, C.X., 2020. The geometry and kinematics of the intersection area of eastern Sichuan and the Dabashan fold-thrust belt. Acta Geol. Sin. 94 (2), 426–438 (in Chinese).

Wu, X.Q., Liu, G.X., Liu, Q.Y., Liu, J.D., Luo, K.P., 2015. xGeochemical characteristics and origin of natural gas in the Xujiahe Formation in Yuanba-Tongnanba area of Sichuan Basin. Oil Gas Geol. 36 (6), 955–974, 10.11743/ogg20150610c (in Chinese).

Wu, X.Q., Liu, Q.Y., Liu, G.X., Ni, C.H., 2019. xGenetic types of natural gas and gas-source correlation in different strata of the Yuanba gas field, Sichuan Basin, SW China. J. Asian Earth Sci. 181, 103906. https://doi.org/10.1016/j.jseaes.2019.103906.

Wu, X.Q., Liu, Q.Y., Zhu, J.H., Li, K., Liu, G.X., Chen, Y.B., Ni, C.H., 2017. Geochemical characteristics of tight gas and gas-source correlation in the Daniudi gas field, the Ordos Basin, China. Mar. Petrol. Geol. 79, 412–425. https://doi.org/10.1016/j.marpetgeo.2016.10.022.

Xu, B., Li, J.H., Xie, D., Wang, X.F., Jian, D., 2011. Distribution of shale gas resources in CNPC exploration area. Special Oil Gas Reservoirs 18 (4), 1–6. https://doi.org/10.3969/j.issn.1006-6535.2011.04.001 (in Chinese).

Xu, Q.H., 2017. Main Controlling Factors of Gas-Water Differential Enrichment and the Geological Model of Sweet Zone, Shilijiahan Area, Ordos Basin. China University of Geosciences, Wuhan (in Chinese).

Yang, T., Zhang, G.S., Liang, K., Zheng, M., Guo, B.C., 2012. The exploration of global tight sandstone gas and forecast of the development tendency in China. Eng. Sci. 14 (6), 64–68. https://doi.org/10.3969/j.issn.1009-1742.2012.06.009 (in Chinese).

Yokoyama, M., Liu, Y.Y., Halim, N., Otofuji, Y.I., 2001. Paleomagnetic study of Upper Jurassic rocks from the Sichuan basin: tectonic aspects for the collision between the Yangtze Block and the North China block. Earth Planet Sci. Lett. 193 (3–4), 273–285. https://doi.org/10.1016/S0012-821X(01)00498-8.

Yu, X.H., Li, S.L., Yang, Z.H., 2015. Discussion on deposition-diagenesis genetic mechanism and hot issues of tight sandstone gas reservoir. Lithologic Reservoirs 27 (1), 1–13. https://doi.org/10.3969/j.issn.1673-8926.2015.01.001 (in Chinese).

Yue, D.L., Wu, S.H., Xu, Z.Y., Xiong, L., Chen, D.X., Ji, Y.L., Zhou, Y., 2018. Reservoir quality, natural fractures, and gas productivity of upper Triassic Xujiahe tight gas sandstones in western Sichuan Basin, China. Mar. Petrol. Geol. 89, 370–386. https://doi.org/10.1016/j.marpetgeo.2017.10.007.

Zeng, L.B., Wang, H.J., Gong, L., Liu, B.M., 2010. Impacts of the tectonic stress field on natural gas migration and accumulation: a case study of the Kuqa Depression in the Tarim Basin, China. Mar. Petrol. Geol. 27 (7), 1616–1627. https://doi.org/10.1016/j.marpetgeo.2010.04.010.

Zhang, F.Q., Wang, Z.L., Song, Y., Zhao, M.J., Liu, S.B., Fang, S.H., 2011. New method of quantitative evaluation on pressurization resulted from tectonic compression in Kuqa depression. J. Univ. Pet., China (Ed. Nat. Sci.) 35 (4), 1–7. https://doi.org/10.3969/j.issn.1673-5005.2011.04.001 (in Chinese).

Zhang, S.Q., Wang, Z.L., Wu, F.L., Gao, L.J., Luo, R.H., Rui, Z.H., 2012. Dynamic analysis on hydrocarbon migration of accumulation periods in low permeability-tight sandstone reservoir. J. Univ. Pet., China (Ed. Nat. Sci.) 36 (4), 32–38. https://doi.org/10.3969/j.issn.1673-5005.2012.04.006 (in Chinese).

Zhang, S.W., Zhang, L.Y., Zhang, S.C., Liu, Q., Zhu, R.F., Bao, Y.S., 2009. Formation of abnormal high pressure and its application in the study of oil-bearing property of lithologic hydrocarbon reservoirs in the Dongying Sag. Chin. Sci. Bull. 54 (23), 4468–4478. https://doi.org/10.1007/s11434-009-0200-9.

Zhao, J.Z., Li, J., Xu, Z.Y., 2017. Advances in the origin of overpressures in sedimentary basins. Acta Pet. Sin. 38 (9), 973–998. https://doi.org/10.7623/syxb201709001 (in Chinese).

Zhao, W.Z., Bian, C.S., Xu, C.C., Wang, H.J., Wang, T.S., Shi, Z.S., 2011. Assessment on gas accumulation potential and favorable plays within the xu-1, 3 and 5 members of the Xujiahe formation in the Sichuan Basin. Petrol. Explor. Dev. 38 (4), 385–393. https://doi.org/10.1016/S1876-3804(11)60041-4.

Zheng, D.Y., Pang, X.Q., Ma, X.H., 2019. Hydrocarbon generation and expulsion characteristics of the source rocks in the third member of the Upper Triassic Xujiahe Formation and its effect on conventional and unconventional hydrocarbon resource potential in the Sichuan Basin. Mar. Petrol. Geol. 109, 175–192. https://doi.org/10.1016/j.marpetgeo.2019.06.014.

Zhou, Z.Z., Zhou, Y.Q., Chen, Y., Bai, Z.H., Mao, C., 2012. A convenient method for obtaining vapor/liquid ratios of fluid inclusions. Geol. Rev. 57 (1), 147–152. https://doi.org/10.3724/SP.J.1011.2011.00181 (in Chinese).

Zou, C., Tao, S., Zhu, R., Yuan, X., Wei, L., Zhang, G., Zhang, X., Gao, X., Liu, L., Xu, C., 2009. Formation and distribution of "continuous" gas reservoirs and their giant gas province: a case from the Upper Triassic Xujiahe Formation giant gas province, Sichuan Basin. Petrol. Explor. Dev. 36 (3), 307–319. https://doi.org/10.1016/S1876-3804(09)60128-2.